ELSEVIER

Chemical Geology 195 (2003) 87–117

CHEMICAL GEOLOGY
INCLUDING
ISOTOPE GEOSCIENCE

www.elsevier.com/locate/chemgeo

Application of Fe isotopes to tracing the geochemical and biological cycling of Fe

Brian L. Beard[a,*], Clark M. Johnson[a], Joseph L. Skulan[a], Kenneth H. Nealson[b], Lea Cox[b], Henry Sun[b]

[a] *Department of Geology and Geophysics, University of Wisconsin-Madison, 1215 West Dayton Street, Madison, WI 53706 USA*
[b] *Jet Propulsion Laboratory, 4800 Oak Grove Drive, Pasadena CA, USA*

Received 20 September 2000; accepted 22 January 2002

Abstract

Over 100 high-precision Fe isotope analyses of rocks and minerals are now available, which constrain the range in δ^{56}Fe values (per mil deviations in $^{56}Fe/^{54}Fe$ ratios) in nature from $-2.50‰$ to $+1.5‰$. Re-assessment of the range of δ^{56}Fe values for igneous rocks, using new ultra-high-precision analytical methods discussed here, indicate that igneous Fe is isotopically homogeneous to $\pm 0.05‰$, which represents an unparalleled baseline with which to interpret Fe isotope variations in nature. All of the isotopic variability in nature lies in fluids, rocks, and minerals that formed at low temperature. Equilibrium (''abiotic'') isotopic fractionations at low temperatures may explain the range in δ^{56}Fe values; experimental measurements indicate that there is a large isotopic fractionation between aqueous Fe(III) and Fe(II) ($\Delta_{Fe(III)-Fe(II)} = 2.75‰$). However, many of the natural samples that have been analyzed have an unquestionable biologic component to their genesis, and the range in δ^{56}Fe values are also consistent with the experimentally measured isotopic fractionations produced by Fe-reducing bacteria.

In this work, we touch on a number of aspects of Fe isotope geochemistry that bear on its application to geochemical problems in general, and biological cycling of metals in particular. We report on new state-of-the-art Fe isotope analytical procedures, which allow precisions of $\pm 0.05‰$ ($^{56}Fe/^{54}Fe$) on samples <300 ng in size. In addition, we discuss the implications of experimental work on Fe isotope fractionations during metabolic processing of Fe by bacteria and the need to take a ''mechanistic'' approach to understanding the pathways in which Fe isotopes may be uniquely fractionated by biology. Additionally, we discuss experimental methods, such as the use of enriched isotope tracers that are necessary to evaluate if experimental isotope exchange reactions are transient kinetic fractionations, equilibrium isotopic exchange reactions, or a combination of both, which can be caused by the complexities of multiple isotope exchange reactions taking place in an experimental system.

Keywords: Fe isotopes; Isotope fractionation; Microbiology; Banded iron formations

1. Introduction

The possibility that Fe isotopes may be fractionated during geochemical cycling, particularly if

* Corresponding author. Tel.: +1-608-262-1806; fax: +1-608-262-0693.
E-mail address: beardb@geology.wisc.edu (B.L. Beard).

0009-2541/02/$ - see front matter © 2002 Elsevier Science B.V. All rights reserved.
doi:10.1016/S0009-2541(02)00390-X

redox changes are involved, has been recognized by geochemists for several decades. The undisputed role of biology in cycling of metals in the near-surface environment (see Nealson and Stahl, 1997) highlights the potential for significant biological influences on Fe isotope fractionation. Recently, analytical methods have been developed for isotope analysis of numerous elements that are heavier than Ca, which have precisions suitable for evaluating naturally occurring, mass-dependent isotope variations (e.g., Marechal et al., 1999; Johnson et al., 1999; Beard and Johnson, 1999; Belshaw et al., 2000). The initial papers to report isotope measurements of these heavy elements were devoted largely to describing analytical methods and to presenting data on geologic specimens that reflect the range of isotope compositions in nature. These investigations are important because they revealed, for the first time, that there are naturally occurring, mass-dependent variations that are resolvable in the isotope compositions of elements heavier than Ca. However, without supporting information concerning the mechanisms of isotope fractionation, the usefulness of these measurements in addressing issues in the geosciences is limited.

In contrast to the limited database for mass-dependent variations of metals, there is a vast database on the isotope variations of elements such as H, C, N, O, and S. Importantly, this database includes a plethora of studies that have been devoted to investigating the mechanisms of isotope fractionation in nature. It is this knowledge of the controlling factors of isotope fractionation that has led to the wide use of stable isotopes in many diverse fields. If the isotope compositions of elements such as Fe, Cu, Zn, and Se are to become a common part of the geochemist's toolbox, studies that take a mechanistic approach to defining the specific pathways of isotope fractionation are required. The methods for these types of studies have been largely developed by the fundamental research in O and C stable isotopes that began in the 1950s, providing an excellent base upon which to develop an understanding of isotopic fractionations of metals.

In a closed system, the record of isotopic fractionation will only be preserved for reactions that did not go to completion; if all the reactant is converted to a product, then mass balance requires that there will be no net isotope effect. In contrast, we have the greatest likelihood of measuring an isotopic difference among materials for reactions that do not proceed to completion. In general, three major types of mass-dependent isotope fractionation are recognized: equilibrium, kinetic, and vital effects. Equilibrium isotope fractionation in the strictest sense only involves isotope exchange between products and reactants that are in chemical equilibrium, where only small free energy differences due to initial isotopic contrasts are the driving forces for isotopic exchange (see reviews by O'Neil, 1986; Criss, 1999; Chako et al., 2001). Isotopic equilibrium may be approached in systems that are also close to chemical equilibrium, such as in the classic case where very slow precipitation of carbonate from solution appears to be accompanied by near equilibrium C and O isotope fractionation (e.g., Trautani et al., 1969). In contrast, for systems that are far from chemical equilibrium, where reaction rates may be quite fast, isotopic fractionations are likely to reflect kinetic effects (see reviews by Cole and Ohmoto, 1986; Criss, 1999; Cole and Chakraborty, 2001). For example, during rapid precipitation of carbonate, the HCO_3^- ion cannot isotopically equilibrate with dissolved CO_2, and differences in the oxygen isotope exchange rates between dissolved CO_2 and HCO_3^-, and HCO_3^- and $CaCO_3$, can produce carbonate minerals that are not in isotopic equilibrium with the solution (e.g., McConnaughey, 1989). In the case of rapid precipitation of carbonate, the oxygen isotope fractionation factor between carbonate and aqueous solution is larger than the equilibrium carbonate aqueous solution fractionation factor for slowly precipitated carbonate (e.g., Kim and O'Neil, 1997), whereas the carbon isotope fractionation factor during rapid precipitation is less than that of the equilibrium value (e.g., Turner, 1982). An important conclusion, therefore, is that the magnitude and sign of a kinetic isotope fractionation will be strongly dependent on initial conditions and the pathway of the reaction, and may be quite far from the equilibrium value.

Meaningful discussions on isotopic variations in natural systems must first start with equilibrium isotope fractionation as a reference point, if for no other reason than nature seems to attain isotopic equilibrium for more frequently, than, for example, in the laboratory, particularly at low temperatures. Distinction between kinetic and equilibrium isotope fractionation is essential, particularly for laboratory experiments at

low temperatures. Although it may be convenient to express equilibrium fractionation as the net result of a forward and backward kinetic fractionation, such a definition is strictly only valid for closed two-component systems involving homogenous isotope exchange (e.g., Northrop and Clayton, 1966; Cole and Ohmoto, 1986). In the case where intermediate species are involved in a reaction, there is a distinct possibility that the intermediate species will be unable to maintain isotopic equilibrium between different reservoirs, producing a net kinetic fractionation (O'Neil, 1986). These kinetic controls on isotope fractionation are important to evaluate in laboratory studies because variations in reaction rates may be quite different in the laboratory as compared to nature. In the case of Fe isotopes, these kinetic effects may be very important during precipitation of iron oxide phases from solutions where, for example, rapid precipitation of hematite produces a large isotopic difference between hematite and aqueous Fe. Additionally, kinetic Fe isotope fractionations have been found between aqueous Fe complexes and anion-exchange resin (Matthews et al., 2001).

In addition to non-equilibrium isotope fractionations that result from differences in the kinetics of isotope exchange reactions, there are non-equilibrium isotope effects that are associated with uni-directional processes such as evaporation or diffusion. An example of this type of fractionation is the variable mass-dependent fractionation that occurs during thermal ionization mass spectrometry. With respect to natural variations in Fe isotope compositions, this kinetic isotope effect has been documented in iron spherules caused by vaporization of these micrometeorites through atmospheric reheating (Herzog et al., 1999), producing very anomalous isotope compositions of up to 50‰. Moreover, kinetic isotope effects associated with volatilization of the solar nebula material may partly be responsible for the 1‰ variations in $^{56}Fe/^{54}Fe$ ratios measured in chondritic meteorites by Zhu et al. (2001).

Urey et al. (1951) coined the term "vital" isotope effect, which may be thought of as a kinetic isotope fractionation that is produced by an organism. Vital effects as recorded in isotope fractionation may be a result of specific metabolic processes, such as the differences in pathways that C3 and C4 plants use in carbon fixation, which produces markedly different $\delta^{13}C$ values (e.g., Schidlowski et al., 1983; Hayes, 2001). Note that vital isotope effects need not be a result of a specific enzymatic process; for example, a kinetic fractionation produced by rapid *biogenic* precipitation of carbonate from ocean water would also be considered a vital effect, as has been well documented for planktonic foraminifera (e.g., Ravelo and Fairbanks, 1995).

In this contribution, we review the Fe isotope system, and develop four main themes. First, we discuss the significant advances in analytical methods that have allowed development of the field of Fe isotope geochemistry. Second, the remarkably restricted range in Fe isotope compositions of igneous rocks is noted, which forms a baseline with which to compare Fe isotope variations in a number of environments. Third, we focus on experimental determinations of Fe isotope fractionation in biological and abiological systems and contrast these results with recent theoretical predictions. Fourth, we conclude with a look at the Fe isotope variations that occur in near-surface natural environments and highlight the need for new studies in specific laboratory and natural systems.

2. Fe isotope analysis methods

Results to date indicate that Fe isotope ratios vary by 3.5‰ in nature. Therefore, it is critical that we obtain measurements of the highest possible precision. Given the narrow range of isotopic variability, an improvement in precision, for example, from ±0.3‰ to ±0.05‰, has dramatic implications for Fe isotope research. High-precision Fe isotope compositions have predominately been measured using two types of instrumentation: thermal ionization mass spectrometry (TIMS) and multi-collector inductively coupled plasma mass spectrometry (MC-ICP-MS; Table 1). Some effort has been made to measure Fe isotope compositions using gas phase electron-impact mass spectrometry by introduction of Fe as $FePF_3$ or as $Fe(CO)_5$ (e.g., Taylor et al., 1993a; Bidinosti and McIntyre, 1967; Sinha et al., personal communication, 2000). Difficulties associated with iron isotope analysis via TIMS include significant and variable mass-dependent fractionation (3–5‰) that occurs during isotopic analysis and the low ionization efficiency of

Table 1
Summary of analytical methods used for Fe isotope analysis

Analysis method	External precision (1 SD)	Sample size	Isotopes measured	Data reporting	References
TIMS, instrumental mass bias corrected using a double spike	0.1‰ per mass (e.g., $^{56}Fe/^{54}Fe$ error is 0.2‰); determined by external reproducibility of samples	4 to 1 μg of Fe	^{54}Fe, ^{56}Fe, ^{57}Fe, ^{58}Fe	Absolute isotope ratios measured, $\delta^{56}Fe$ values reported relative to average iron isotope composition of igneous rocks	Beard and Johnson, 1999; Johnson and Beard, 1999; Beard et al., 1999; Bullen et al., 2001
TIMS instrumental mass bias corrected empirically based on analysis of standards run at same conditions as samples	1–2‰ per mass determined by external reproducibility of samples	0.1 to 6 μg of Fe	^{54}Fe, ^{56}Fe, ^{57}Fe, ^{58}Fe	Absolute isotope ratios measured	Dixon et al., 1993; Walczyk, 1997
MC-ICP-MS Argide interferences minimized by use of desolvating nebulizer	$^{56}Fe/^{54}Fe \pm 0.15$‰, $^{57}Fe/^{56}Fe \pm 0.30$‰, errors assigned to represent external precision of samples	6 μg of Fe	^{54}Fe, ^{56}Fe, ^{57}Fe	Isotope ratios reported relative to an ultra-pure metal from Johnson Mathey	Anbar et al., 2000
MC-ICP-MS HCl matrix used to minimize ArN, very large quantities of Fe used to make isobar interferences small	$^{54}Fe/^{57}Fe \pm 0.03$‰; error assigned from reproducibility of ultra-pure metal standards	20 μg of Fe	^{54}Fe, ^{56}Fe, ^{57}Fe	Isotope ratios reported relative to an ultra-pure metal from IRMM (IRMM-014); Fe isotope compositions reported as $\varepsilon^{57}Fe$ which is approximately equal to $15 \times \delta^{56}Fe$, assuming the same reference reservoir	Zhu et al., 2000, 2001; Belshaw et al., 2000
MC-ICP-MS, collision cell with H_2 gas used to eliminate ArO and ArN, and minimize ArOH isobar	$^{54}Fe/^{56}Fe \pm 0.05$‰, $^{57}Fe/^{56}Fe \pm 0.05$‰, $^{54}Fe/^{57}Fe \pm 0.07$‰, errors determined by reproducibility of sample analyses	0.3 to 0.1 μg of Fe	^{54}Fe, ^{56}Fe, ^{57}Fe	Relative isotope ratios measured, compared relative to an ultra-pure metal from High Purity Standards; $\delta^{56}Fe$ values are reported relative to the average iron isotope composition of igneous rocks	This study

iron at $\sim 1 \times 10^{-5}$ (Völkening and Papanastassiou, 1989). Despite these challenges, analysis by TIMS produced the first high-precision Fe isotope ratio measurements that preserve naturally occurring, mass-dependent variations (Beard and Johnson, 1999; Table 1). Iron isotope analysis by MC-ICP-MS circumvents many of the problems associated with TIMS analysis because instrumental mass bias may be very constant (although much greater in magnitude than TIMS, at 30–50 ‰ /mass), and the ionization efficiency is very high ($\sim$ 0.1–0.5%). However, MC-ICP-MS isotope analysis produces other challenges because of isobar interferences that are introduced by the Ar plasma at ^{54}Fe from $^{40}Ar^{14}N$, at ^{56}Fe from $^{40}Ar^{16}O$, and ^{57}Fe from $^{40}Ar^{16}OH$. In addition, in natural samples, variable matrices may produce interferences from Ca, Cr, and Ni ($^{40}Ca^{16}O$ for ^{56}Fe, $^{40}Ca^{16}OH$ for ^{57}Fe, ^{54}Cr for ^{54}Fe, and ^{58}Ni for ^{58}Fe, to name just a few).

Several approaches have been taken to circumvent argide isobar problems (Table 1). Most methods have attempted to minimize argide interferences through the choice of acid matrix, use of a desolvating nebulizer, and by use of large quantities of Fe ($\sim$ 5–25 μg of Fe) (Table 1); additional approaches include running under ‘‘cool’’ plasma conditions, although this results in a significant loss in sensitivity. It is difficult to assess fully the true reproducibility that various analytical approaches are capable of since few studies have extensively reported the precision of replicate analyses of natural samples obtained over a long period, under significantly different running conditions. Precisions reported for duplicate analyses of the same ultra-pure standard solution fail to provide a full assessment of true external reproducibility. Here we report on the MC-ICP-MS methods we have used that provide an external reproducibility on natural samples of $\pm$ 0.05 ‰ (1 SD) for $^{56}Fe/^{54}Fe$ ratios in $\leq$ 5 nmol ($\leq$ 300 ng) size samples.

The MC-ICP-MS methods and instrumentation in our laboratory completely eliminate some argide interferences (ArO and ArN) and significantly minimize others (ArOH). Such techniques are important for ultra-high-precision analyses of small samples, because argide interferences can be highly variable in their isotopic ratios (varying over several hundred per mil over an hour period; B. Beard and C. Johnson, unpublished data), and peak-centering errors can be significant when large interferences are present. For example, our tests on several instruments show that conventional MC-ICP-MS measurements on 300 ppb Fe solutions are limited to a precision of approximately of $\pm$ 0.3 ‰ for $^{56}Fe/^{54}Fe$ and $\pm$ 0.6 ‰ for $^{57}Fe/^{54}Fe$ even for argide interferences occurring at levels of only a few mV because of variability in the isotopic composition of the interference. Higher precision data can only be obtained at significantly higher Fe contents; this effect has been well demonstrated by Belshaw et al. (2000).

Data reported here were obtained using a Micromass *IsoProbe* MC-ICP-MS, a single focusing instrument with a sector-style magnet, which critically includes a collision cell. A collision gas, such as Ar, is inlet into the cell at a flow rate of $\sim$ 1 ml/min. The collision gas thermalizes the ion beam, reducing the ion energy spread to $\sim$ 1 eV, allowing the mass analyzer to produce flat-topped peak shapes. Additionally, it is possible to also add a reactive collision gas, such as H_2, that eliminates or greatly reduces molecular isobars such as ArN. Optimization of plasma and collision cell gases, including complete removal of water and organic contaminants in the interface region, results in near complete removal of argide interferences on the Fe mass spectrum (Fig. 1). In our experience, the most difficult interference to remove is $^{40}Ar^{16}OH$, which can only be identified unambiguously from high-resolution mass scans, and is isobaric with the low-abundance isotope ^{57}Fe. Production of $^{40}Ar^{16}OH$ in our instrument is not produced by our use of H_2 in the collision gas mixture because the $^{40}Ar^{16}OH$ ion intensity is invariant over a wide range of collision gas Ar/H ratios. We do not believe that FeH generation is a problem because $^{57}Fe/^{56}Fe$ isotope measurements do not show nonlinear isotope effects with variable Fe concentrations.

Difficulties in measuring precise ^{57}Fe abundances notwithstanding, we stress the importance of measuring at least two Fe isotope ratios (e.g., $^{56}Fe/^{54}Fe$ and $^{57}Fe/^{54}Fe$) as an internal data quality check. In our MC-ICP-MS work, we have decided to not attempt high-precision ^{58}Fe measurements for most samples due to the advantages of using Ni cones, although the very large mass dispersion of the *IsoProbe* allows simultaneous measurement of mass 52 to 60, thus covering the Fe mass spectrum and Cr and Ni isobars. We note that extraterrestrial work may require precise

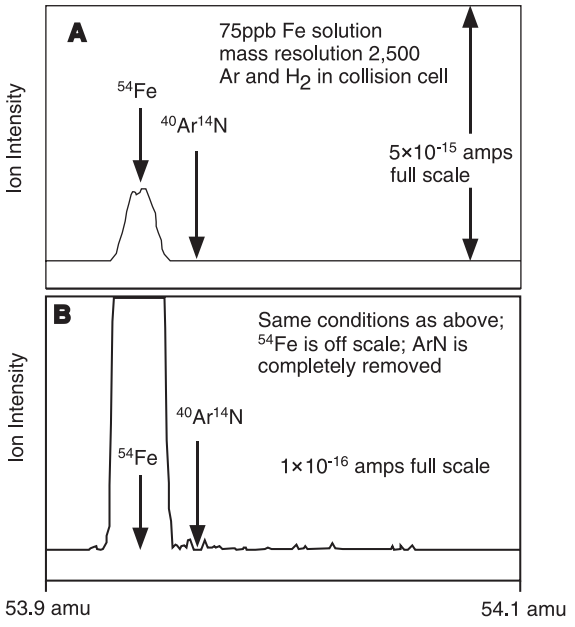

Fig. 1. Peak scan (plot of increasing magnetic field strength versus ion intensity) of a part of the Fe mass spectrum at high mass resolution (2500) using an ion-counting Daly detector on the Micromass *IsoProbe*. A resolving power of 2500 is sufficient to resolve Fe metal ions from their Argide interferences. (A) Peak scan across ^{54}Fe mass spectrum, with the position of $^{40}Ar^{14}N$ shown; ion intensity at full scale is 5×0^{-15} A. (B) Same plot as in A, but full scale is 1×10^{-16} A, and the position of $^{40}Ar^{14}N$ is indicated by the arrow. A mixture of Ar and H_2 gas in the collision cell completely removes ArN.

measurements of ^{58}Fe (e.g., Völkening and Papanastassiou, 1989).

Iron isotope measurements were made by simultaneous collection of ^{54}Fe, ^{56}Fe, and ^{57}Fe, and monitoring of ^{52}Cr for isobaric interference of ^{54}Cr on ^{54}Fe. Chromium interference was corrected using $^{54}Cr/^{52}Cr = 0.0282$ (Beard and Johnson, 1999) but was generally less than 0.002% on the $^{54}Fe/^{56}Fe$ ratio. We analyzed Fe standard solutions that were doped with various Cr contents and there is no bias in the measured Fe isotope ratios between the Cr doped and Cr-free standard solutions over a range of Cr/Fe ratios (Cr contents up to 0.2 ppb).

Samples were introduced in a weak HNO_3 acid matrix using a self-aspirating, low-flow (either a 100 or 50 μl/min) desolvating nebulizer (*Aridus*, made by Cetac). A standard solution is measured before and after every analysis to correct for instrumental mass bias changes. We investigated using Ni and Cu as normalizing elements (following the approach of Marechal et al., 1999) but found that a sample-standard analysis approach produced higher precision data because mass bias relations among the Fe isotopes did not follow those of Ni and Cu during an analysis. Similar results have been found by other workers (Belshaw et al., 2000). Sample concentrations were approximately 300 ppb Fe, which produced a 3×10^{-10} A ^{56}Fe signal; all masses except ^{56}Fe are measured on Faraday collectors using 10^{11} Ω resistors; ^{56}Fe is measured using a 10^{10} Ω resistor.

Our methods for chemical separation of Fe from complex geologic and biologic matrixes are reported in Beard and Johnson (1999), Beard et al. (1999), and Skulan et al. (2002). Briefly, once a sample is dissolved, Fe is separated from other cations using anion-exchange resin (Bio-Rad AG 1X4 200–400 mesh) and HCl (e.g., Strelow, 1980). MC-ICP-MS analysis generally requires better chemical separation methods than TIMS analysis because TIMS can make use of differences in ionization temperatures of isobaric interfering elements by burning these elements off the filament during warm-up (Beard and Johnson, 1999). We tested both our original and revised ion-exchange column separations using the ultra-high-precision capabilities of our MC-ICP-MS instrument to determine if any isotopic fractionation is introduced; this is of particular concern considering the recent work on Fe isotope fractionation using ion-exchange resin, as reported by Anbar et al. (2000). Tests included processing ultra-pure Fe standards that had been doped with other cations (Ca, Mg, Na, and Cr), and the isotopic compositions of separated Fe

Note to Table 2:
All Fe isotope measurements made using the U.W. Micromass *IsoProbe*. 2 SE is two standard errors calculated from in-run statistics. 1 SD is one standard deviation calculated from the average of two or more analyses of the same sample; 2 SE is used if only one analysis is available. Average of individual dissolution represents analyses on the sample dissolution, which provides a robust estimate of the precision of the mass spectrometry measurements. Diss 1, Diss 2, Diss 3 indicate replicate dissolution of different splits from a whole rock powder; the reproducibility of these analyses provides a robust estimate of the complete external precision of Fe isotope analyses.

Table 2
Fe isotope compositions of terrestrial igneous rocks

		Individual analyses of solution				Average of individual dissolution				Grand average of igneous rock			
		δ^{56}Fe	2 SE	δ^{57}Fe	2 SE	δ^{56}Fe	1 SD	δ^{57}Fe	1 SD	δ^{56}Fe	1 SD	δ^{57}Fe	1 SD
Ultramafic rocks													
PCC-1 Peridotite	Diss 1	−0.04	0.10	−0.10	0.06	−0.05	0.02	−0.06	0.04	−0.06	0.06	−0.09	0.06
(USGS Standard)		−0.03	0.08	−0.01	0.05								
		−0.07	0.04	−0.06	0.04								
	Diss 2	−0.13	0.06	−0.17	0.04	−0.12	0.01	−0.17	0.00				
		−0.12	0.05	−0.17	0.03								
	Diss 3	−0.01	0.05	−0.06	0.05	−0.01	0.05	−0.06	0.05				
Meta komatiite		−0.12	0.08	−0.17	0.04	−0.02	0.08	−0.07	0.09	−0.02	0.08	−0.07	0.09
PS 7.9-87		0.04	0.04	−0.01	0.02								
		0.00	0.05	−0.03	0.03								
Peridotite Pi-2-6		−0.10	0.09	−0.12	0.06	−0.10	0.03	−0.10	0.02	−0.10	0.03	−0.10	0.02
Olivine mineral sep.		−0.14	0.07	−0.09	0.05								
		−0.07	0.06	−0.10	0.04								
Continental basaltic rocks													
BCR-1 Basalt	Diss 1	−0.07	0.05	−0.15	0.03	0.02	0.07	0.02	0.14	0.00	0.04	0.01	0.02
(USGS Standard)		−0.03	0.05	−0.05	0.03								
		0.08	0.04	0.23	0.03								
		0.06	0.05	0.00	0.03								
		0.06	0.04	0.06	0.02								
	Diss 2	0.06	0.05	0.04	0.04	0.03	0.04	0.03	0.12				
		−0.02	0.08	−0.09	0.04								
		0.05	0.09	0.14	0.05								
	Diss 3	−0.04	0.06	−0.01	0.04	−0.04	0.06	−0.01	0.04				
NW USA Basalt 1959		−0.05	0.07	−0.05	0.04	−0.01	0.05	0.02	0.11	−0.01	0.05	0.02	0.11
		−0.03	0.07	−0.03	0.04								
		0.04	0.23	0.14	0.07								
NW USA Basalt		0.03	0.09	0.01	0.07	0.03	0.03	−0.01	0.02	0.03	0.03	−0.01	0.02
UMAT-1		0.07	0.04	−0.01	0.03								
		0.01	0.10	−0.01	0.06								
		0.00	0.06	−0.04	0.03								
NW USA Basalt		−0.03	0.05	−0.01	0.03	−0.03	0.00	−0.01	0.01	−0.03	0.00	−0.01	0.01
H-8-91		−0.03	0.06	−0.02	0.04								
NW USA Basalt		0.02	0.06	0.00	0.03	−0.01	0.03	0.02	0.03	−0.01	0.03	0.02	0.03
HSR-16		−0.03	0.07	0.04	0.05								
SW USA Basalt		−0.02	0.10	0.02	0.06	0.03	0.05	0.08	0.05	0.03	0.05	0.08	0.05
Pi-2-101		0.02	0.06	0.10	0.03								
		0.08	0.05	0.11	0.02								
Mid-ocean ridge basalts													
Mid-Pacific Ridge		−0.01	0.11	0.11	0.07	0.00	0.00	−0.02	0.12	0.00	0.00	−0.02	0.12
K42a-D206F		0.00	0.05	−0.04	0.04								
		−0.01	0.05	−0.14	0.04								
Mid-Pacific Ridge		0.13	0.06	0.15	0.03	0.02	0.16	0.05	0.14	0.02	0.16	0.05	0.14
K71a-D130H		−0.09	0.06	−0.04	0.04								
Mid-Pacific Ridge		0.09	0.08	0.09	0.04	0.05	0.07	0.02	0.09	0.05	0.07	0.02	0.09
Amph D4		0.08	0.08	0.05	0.04								
		−0.03	0.05	−0.08	0.04								
Mid-Pacific		0.08	0.07	0.09	0.04	−0.02	0.07	−0.01	0.07	−0.02	0.07	−0.01	0.07
Ridge P4G		−0.11	0.11	−0.05	0.06								
		−0.03	0.06	−0.06	0.04								
		−0.02	0.04	−0.02	0.03								

(continued on next page)

Table 2 (*continued*)

		Individual analyses of solution				Average of individual dissolution				Grand average of igneous rock			
		δ^{56}Fe	2 SE	δ^{57}Fe	2 SE	δ^{56}Fe	1 SD	δ^{57}Fe	1 SD	δ^{56}Fe	1 SD	δ^{57}Fe	1 SD
Mid-ocean ridge basalts													
Indian Ocean Ridge		0.04	0.10	0.10	0.04	0.01	0.04	0.02	0.12	0.01	0.04	0.02	0.12
VG5262		−0.02	0.05	−0.07	0.03								
Famous Ridge 534-2-1		0.09	0.06	0.14	0.03	0.12	0.04	0.18	0.05	0.12	0.04	0.18	0.05
		0.16	0.08	0.23	0.04								
		0.12	0.05	0.17	0.04								
Famous 528-3		0.07	0.07	0.10	0.04	0.04	0.07	0.01	0.15	0.04	0.07	0.01	0.15
		−0.04	0.05	−0.17	0.03								
		0.09	0.05	0.09	0.04								
Galapagos Ridge E-76		−0.04	0.08	0.02	0.04	0.00	0.06	0.03	0.02	0.00	0.06	0.03	0.02
		0.04	0.08	0.05	0.04								
Galapagos Ridge E-1		0.05	0.07	0.18	0.05	0.05	0.01	0.10	0.12	0.05	0.01	0.10	0.12
		0.04	0.05	0.02	0.03								
Galapagos Ridge E-234		−0.07	0.06	−0.09	0.04	−0.03	0.05	−0.07	0.04	−0.03	0.05	−0.07	0.04
		0.00	0.06	−0.04	0.04								
Galapagos Ridge FL-27		0.15	0.09	0.25	0.04	0.09	0.05	0.14	0.10	0.09	0.05	0.14	0.10
		0.07	0.10	0.10	0.04								
		0.06	0.05	0.06	0.03								
Ocean island basalts (OIB)													
Hawaii-Koolau 6308		−0.04	0.04	−0.01	0.04	0.01	0.06	0.04	0.09	0.01	0.06	0.04	0.09
		0.09	0.03	0.13	0.03								
		−0.05	0.05	−0.05	0.04								
		0.04	0.05	0.10	0.04								
Hawaii-Koolau K001	Diss 1	0.01	0.04	0.01	0.03	0.03	0.03	0.01	0.01	−0.03	0.08	−0.03	0.06
		0.05	0.04	0.02	0.03								
	Diss 2	−0.15	0.09	−0.12	0.05	−0.09	0.08	−0.07	0.07				
		−0.04	0.06	−0.02	0.03								
Hawaii-Koolau K0017A	Diss 1	0.02	0.05	−0.06	0.04	0.01	0.01	−0.06	0.00	−0.04	0.08	−0.07	0.01
		0.00	0.06	−0.05	0.04								
	Diss 2	−0.10	0.12	−0.07	0.06	−0.10	0.00	−0.08	0.01				
		−0.10	0.05	−0.09	0.03								
Hawaii-Koolau K0030	Diss 1	0.04	0.04	−0.07	0.04	0.03	0.02	0.02	0.13	−0.04	0.09	−0.04	0.09
		0.02	0.05	0.11	0.04								
	Diss 2	−0.13	0.08	−0.11	0.05	−0.10	0.04	−0.10	0.02				
		−0.07	0.03	−0.08	0.04								
Hawaii-Mauna Kea		0.02	0.05	0.08	0.04	0.03	0.04	0.04	0.06	0.03	0.04	0.04	0.06
HSDP R166		0.07	0.05	0.08	0.04								
		−0.01	0.05	−0.02	0.03								
Hawaii-Mauna Kea		0.02	0.05	0.02	0.03	0.01	0.02	−0.02	0.06	0.01	0.02	−0.02	0.06
HSDP R177		−0.01	0.05	−0.07	0.04								
Hawaii-Mauna Kea		−0.04	0.05	−0.04	0.04	−0.04	0.05	−0.04	0.04	−0.04	0.05	−0.04	0.04
HSDP R303													
Society Is. -Tahaa 73-186		0.01	0.08	−0.14	0.05	−0.03	0.07	−0.07	0.09	−0.03	0.07	−0.07	0.09
		−0.08	0.06	−0.01	0.06								
Society Is.-Tahaa 73-192		−0.02	0.06	0.02	0.04	0.06	0.12	0.04	0.14	0.06	0.12	0.04	0.14
		0.19	0.10	0.19	0.05								
		0.00	0.06	−0.09	0.04								
Society Is.-Tahiti 74-416		0.00	0.06	0.00	0.03	−0.03	0.04	−0.06	0.09	−0.03	0.04	−0.06	0.09
		−0.06	0.06	−0.13	0.05								
Kergulen Is.-OPD-119		−0.07	0.10	−0.10	0.06	−0.11	0.06	−0.16	0.08	−0.11	0.06	−0.16	0.08
		−0.09	0.10	−0.14	0.05								
		−0.18	0.04	−0.25	0.03								

Table 2 (*continued*)

		Individual analyses of solution				Average of individual dissolution				Grand average of igneous rock			
		δ^{56}Fe	2 SE	δ^{57}Fe	2 SE	δ^{56}Fe	1 SD	δ^{57}Fe	1 SD	δ^{56}Fe	1 SD	δ^{57}Fe	1 SD
Ocean island basalts (OIB)													
Kergulen Is.-GM92-29	Diss 1	0.14	0.06	0.14	0.06	0.12	0.02	0.16	0.03	0.08	0.05	0.15	0.02
		0.11	0.05	0.19	0.04								
		0.12	0.06	0.14	0.04								
	Diss 2	0.00	0.05	0.12	0.03	0.05	0.07	0.13	0.03				
		0.10	0.05	0.15	0.04								
Kergulen Is.-GM92-48	Diss 1	0.01	0.05	0.07	0.03	0.01	0.05	0.07	0.03	−0.01	0.02	0.04	0.05
	Diss 2	−0.08	0.09	−0.05	0.06	−0.02	0.07	0.00	0.07				
		0.03	0.04	0.05	0.04								
Kergulen Is.-92-58	Diss 1	−0.08	0.04	−0.04	0.04	−0.04	0.05	0.00	0.06	−0.02	0.03	0.02	0.03
		0.00	0.05	0.04	0.04								
	Diss 2	0.05	0.09	0.09	0.05	0.01	0.06	0.04	0.08				
		−0.03	0.05	−0.02	0.03								
Continental silicic igneous rocks													
Rhyolite, biotite		−0.02	0.07	0.07	0.04	−0.04	0.03	−0.01	0.06	−0.04	0.03	−0.01	0.06
phenocryst FG 1		−0.08	0.08	−0.03	0.04								
		−0.03	0.05	−0.07	0.03								
		−0.02	0.07	0.00	0.04								
Rhyolite, BP9220B		−0.13	0.08	−0.14	0.04	−0.07	0.06	−0.08	0.07	−0.07	0.06	−0.08	0.07
		−0.08	0.07	−0.08	0.04								
		−0.01	0.06	−0.01	0.03								
Dacite, biotite		−0.04	0.07	−0.09	0.03	−0.02	0.03	−0.07	0.03	−0.02	0.03	−0.07	0.03
phenocryst FG 3B		0.02	0.06	−0.03	0.03								
		0.01	0.05	−0.09	0.04								
		−0.05	0.05	−0.06	0.02								
Granite, biotite		0.06	0.09	0.14	0.06	−0.03	0.07	−0.05	0.14	−0.03	0.07	−0.05	0.14
separate Q82J-8		−0.02	0.09	−0.07	0.05								
		−0.09	0.07	−0.19	0.04								
		−0.07	0.05	−0.09	0.03								
Granite, biotite		0.01	0.08	0.11	0.05	−0.08	0.08	−0.09	0.14	−0.08	0.08	−0.09	0.14
separate Q82J-33		−0.04	0.06	−0.10	0.04								
		−0.17	0.09	−0.22	0.03								
		−0.13	0.11	−0.15	0.06								
Basaltic Andesite		0.04	0.09	0.14	0.06	0.00	0.09	0.04	0.14	0.00	0.09	0.04	0.14
Amphibole		−0.10	0.05	−0.12	0.02								
phenocryst Fg7		0.06	0.08	0.10	0.04								
Quartz Latite, QL-1		0.02	0.09	−0.02	0.05	0.02	0.09	−0.02	0.05	0.02	0.09	−0.02	0.05
GSP-1 Granodiorite		−0.01	0.08	−0.05	0.04	0.02	0.04	−0.03	0.03	0.02	0.04	−0.03	0.03
(USGS Standard)		0.05	0.06	0.00	0.04								
AGV-1 Andesite	Diss 1	0.03	0.06	−0.05	0.04	0.03	0.01	0.01	0.08	0.04	0.01	0.03	0.03
(USGS Standard)		0.04	0.05	0.06	0.04								
	Diss 2	0.04	0.06	0.05	0.04	0.04	0.06	0.05	0.04				
RGM-1 Rhyolite		0.09	0.11	0.18	0.05	0.09	0.11	0.18	0.05	0.09	0.11	0.18	0.05
(USGS Standard)													
STM-1 Nepheline Syenite		0.11	0.10	0.13	0.06	−0.05	0.23	−0.05	0.26	−0.05	0.23	−0.05	0.26
(USGS Standard)		−0.22	0.06	−0.23	0.06								
G-2 Granite		−0.07	0.08	−0.01	0.05	−0.02	0.07	0.02	0.04	−0.02	0.07	0.02	0.04
(USGS Standard)		0.03	0.08	0.05	0.04								

were identical to the results of tests using ultra-pure standards that contained only Fe. Test solutions had Ca/Fe and Cr/Fe weight ratios of 1 and 0.02, respectively, or Ca/Fe, Mg/Fe, Na/Fe, and Cr/Fe weight ratios of 0.75, 0.75, 0.4, and 0.02, respectively. The Fe isotope compositions before and after ion-exchange separation are identical within the uncertainty of our MC-ICP-MS measurements at ± 0.05 ‰, over a range of Fe contents (10 to 10,000 μg of Fe processed), as well as during multiple passes (up to three) through the columns. As an additional test on our analytical separation methods, we have replicated nine whole rock samples by dissolution of different whole rock splits. Agreement between these complete replicate analyses is ± 0.05 ‰ (1 SD) (Table 2), which is the limit of external precision of our mass spectrometry analysis based on replicate analyses of ultra-pure standard solutions (see below).

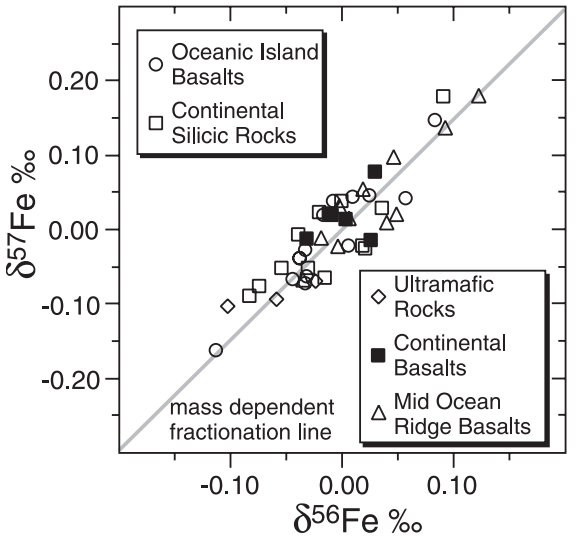

Fig. 2. Plot of measured δ^{56}Fe versus δ^{57}Fe values of igneous rocks. Plotted Fe isotope values are average values calculated from the data reported in Table 2.

3. A homogenous terrestrial baseline for Fe isotopes

In our initial report on Fe isotopes, we noted the striking constancy of the Fe isotope composition of igneous rocks, where the average δ^{56}Fe value of 15 terrestrial igneous rocks and five lunar basalts was 0 ± 0.25 ‰ (Beard and Johnson, 1999). The homogenous Fe isotope composition of igneous rocks led us to propose that Fe isotope variations should be reported relative to this baseline, where:

$$\delta^{56}\text{Fe}‰ = (^{56}\text{Fe}/^{54}\text{Fe}_{\text{SAMPLE}} / ^{56}\text{Fe}/^{54}\text{Fe}_{\text{E-M SYSTEM}} - 1)10^3$$

and the ^{56}Fe/^{54}Fe$_{\text{E-M SYSTEM}}$ is the average of these lunar and terrestrial igneous rocks.

This definition provided a useful reference composition from which to identify anomalous Fe isotope relationships relative to a bulk-earth composition. Our approach is similar to that used with other stable isotope systems wherein isotopic deviations are defined relative to a large reservoir, such as the use of Standard Mean Ocean Water (SMOW) for the oxygen isotope system.

We reanalyzed 14 of these terrestrial igneous rocks using our MC-ICP-MS instrument, using the same solutions that were previously measured by TIMS. In addition, we analyzed 32 other igneous rocks. This suite of igneous rocks includes 3 ultramafic rocks, 6 continental basalts, 11 mid-ocean ridge basalts (MORB), 14 oceanic island basalts (OIB), and 12 continental silicic igneous rocks. The constancy of "igneous Fe" is even more dramatic than we initially reported; the new mean δ^{56}Fe value of terrestrial igneous rocks is 0.00 ± 0.05 ‰ (1σ; Table 2). Interestingly, on a two Fe isotope plot (Fig. 2), the measured Fe isotope composition of igneous rocks may reveal a very slight mass-dependent variation; this may reflect very small deviations in Fe isotope compositions of the samples or may reflect a small-magnitude "second-order" mass bias effect in the MC-ICP-MS measurements. There may be some very small differences in the Fe isotope composition among these different igneous rocks, where, for example, the average δ^{56}Fe value of the three ultramafic rocks is -0.06 ‰, and the average δ^{56}Fe value of the 11 MORB is $+0.03$ ‰. However, these differences cannot be resolved at the 2σ level (± 0.10 ‰).

The extreme constancy in the isotopic composition of igneous or "bulk-earth" Fe dramatically contrasts with almost all other stable isotope systems. For example, δ^{18}O values of similar composition igneous rocks vary by 5–10 ‰ (e.g., Criss, 1999). This result has important implications for tracing the geochemical

cycling of Fe. It is reasonable in environments where the source of Fe is "lithologic" to assume that the initial δ^{56}Fe value of the source Fe was zero. In contrast, the starting compositions for other stable isotope systems used to trace biochemical cycling may be quite variable, making identification of the biological or "vital" component more difficult. For example, interpretation of the δ^{18}O values of biogenic minerals must address the fact that the δ^{18}O values of meteoric and hydrothermal fluids may vary from −50‰ to +10‰ (e.g., Criss, 1999).

3.1. Data reporting and reference standards

The potential for confusion in comparing data among laboratories is great when new isotope systems are developed. We favor reporting Fe isotope variations in per mil notation (parts per 10^3), following other stable isotope systems, using both δ^{56}Fe (deviations in ^{56}Fe/^{54}Fe, as noted above) and δ^{57}Fe (deviations in ^{57}Fe/^{54}Fe). Variations in ^{57}Fe/^{56}Fe can be noted as δ^{57}Fe/^{56}Fe. So far, work at the University of Wisconsin-Madison, the US Geological Survey, and the University of Rochester have used the per mil notation (Beard and Johnson, 1999; Johnson and Beard, 1999; Beard et al., 1999; Mandernack et al., 1999; Anbar et al., 2000; Bullen et al., 2001; Brantley et al., 2001). Although δ^{57}Fe for natural samples was defined as the deviation in ^{57}Fe/^{56}Fe in an early study from the U.S.G.S. lab (Bullen and McMahon, 1998), this approach was discontinued. Work at Oxford University has used the ε notation (parts per 10^4) for ^{57}Fe/^{54}Fe ratios (Belshaw et al., 2000; Zhu et al., 2000, 2001; Matthews et al., 2001). Assuming normalization to an identical reference reservoir (see below), an ε^{57}Fe value of +10.0, as defined by the Oxford Group, would be approximately equal to a δ^{56}Fe value of +0.67, as defined here.

We recommend that all δ^{56}Fe and δ^{57}Fe values be normalized to average igneous Fe and that interlaboratory comparisons be made through the use of an Fe isotope reference material, such as IRMM-014. The IRMM-014 Fe isotope standard is available from the Institute for Reference Materials and Measurements, Belgium, and is described by Taylor et al. (1992, 1993b). The δ^{56}Fe value of IRMM-014 relative to the igneous Fe baseline is -0.09 ± 0.05‰. Agreement on a specific solution standard is important, given the isotopic variability we have found in different Fe metal standards (Fig. 3). The three ultra-pure Fe standards that we routinely analyze include two internal laboratory standards purchased from Johnson

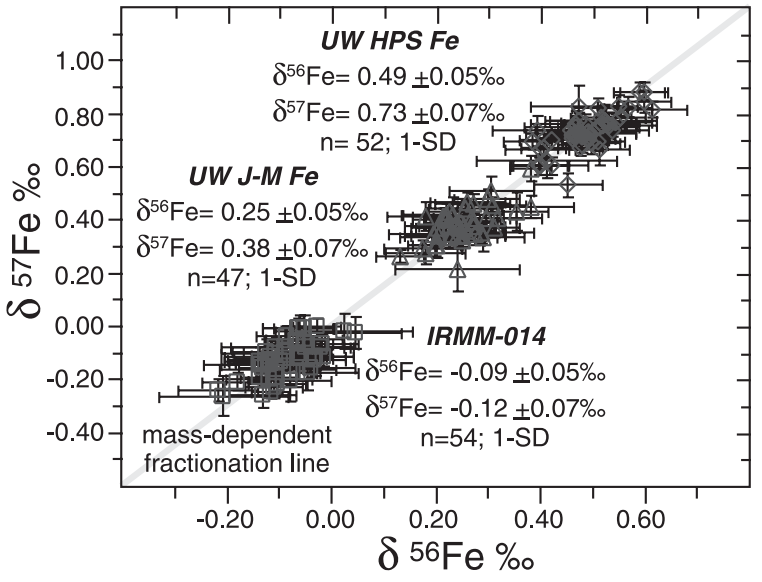

Fig. 3. Plot of measured δ^{56}Fe versus δ^{57}Fe values of three ultra-pure metal standards. Plotted Fe isotope values are individual analyses collected from June 2000 to July 2001; error bars are two standard errors from the internal run statistics (30 ratios).

Mathey (UW J-M Fe) and High Purity Standards (UW HPS Fe); the third standard is IRMM-014. The measured Fe isotope composition of these three standards during the course of this study were: UW J-M Fe, $\delta^{56}Fe = 0.25 \pm 0.05$ ‰ $^{57}Fe = 0.39 \pm 0.07$ ‰ (1 SD, $n = 47$); UW HPS Fe, $\delta^{56}Fe = 0.49 \pm 0.05$ ‰ and $\delta^{57}Fe = 0.74 \pm 0.07$ ‰ (1 SD, $n = 52$); and IRMM-014, $\delta^{56}Fe = -0.09 \pm 0.05$ ‰ and $\delta^{57}Fe = -0.11 \pm 0.07$ ‰ (1 SD, $n = 54$). It is uncertain if the variability in these different Fe metal standards is caused by industrial processing (similar to the volatilization effects documented by Russell et al., 1978 for Ca isotopes), or if this is caused by natural variations in the source of the raw Fe material (such as Banded Iron Formations).

Accuracy of Fe isotope compositions is more difficult to address. The accuracy of the Fe isotope composition of the IRMM-014 standard was established by careful gravimetric analysis but the analytical uncertainties are ~1 ‰ /mass (Taylor et al., 1992), which are not precise enough to allow conversion of measured MC-ICP-MS ratios to true ratios at a precision of ±0.05 ‰. We are therefore left with reporting Fe isotope compositions on a relative basis.

4. Experimental and theoretical constraints on Fe isotope variations

There are now several experimental studies that provide a glimpse of the magnitude and controlling factors of Fe isotope fractionation, including those focused on assessing the influence of biologic activity (e.g., Beard et al., 1999; Mandernack et al., 1999; Brantley et al., 2001; and this study, see below), as well as isotopic fractionation in abiologic or inorganic systems (Anbar et al., 2000; Bullen et al., 2001; Matthews et al., 2001; Johnson et al., 2002; Skulan et al., 2002). In addition, Fe isotope fractionation factors have been calculated for various mineral phases and aqueous species based on spectroscopic data (Polyakov and Mineev, 2000; Schauble et al., 2001).

4.1. Biological fractionation

There are three experimental studies available to evaluate "biologically produced" Fe isotope fractionation, involving (a) Fe-reducing bacteria (Beard et al., 1999; this study), (b) mineral dissolution in the presence of organic ligands (Brantley et al., 2001), and (c) magnetotactic bacteria (Mandernack et al., 1999). Initial results obtained using the Fe-reducing bacteria *Shewanella alga* cultured on ferrihydrite using a growth medium containing yeast extract showed that the $\delta^{56}Fe$ value of bacterially reduced Fe is about 1.3 ‰ lower than that of the Fe(III) substrate (Beard et al., 1999), and led to our proposal that Fe isotopes may prove to be a useful "biosignature." These experiments were not without difficulties, however, primarily because abiotic dissolution of ferrihydrite was a problem in the rich growth media that was used, and an unusually low $\delta^{56}Fe$ value appeared to be a blank component in the yeast extract (Beard et al., 1999).

New experiments reported here used a hematite substrate and a minimal-salts growth medium, which eliminates abiotic dissolution issues. Hematite (0.5 g Fe_2O_3) was added to 2.3 l of a minimal-salts growth medium (Myers and Nealson, 1988) and an inoculum of *S. alga* (3.3×10^8 cells/ml, determined by plate count) was added. The carbon source in this medium is lactate with amino acids, added in μM concentrations. An identical abiological control experiment was prepared that was not inoculated with cells. The inoculated solution and the abiological control were sampled at 7, 15, 27, 41, 63, and 84 days following inoculation; Fe(II) contents were measured using *Ferrozine* (Stookey, 1970) at these time intervals. The aqueous Fe concentration of the abiological control was below the detection limits of the *Ferrozine* method (<2 μM Fe). In the experiment with cells, the aqueous Fe concentration increased rapidly in the first 30 days and then Fe contents leveled (Fig. 4A). After 84 days, the experiment with cells was harvested. Based on a mass balance using the measured Fe concentration in the growth media, this corresponds to 1.56% dissolution of the hematite substrate. The cells and hematite were separated from the aqueous Fe by centrifuge. The Fe isotope compositions of the aqueous Fe, reacted hematite, and stock hematite were measured using the TIMS double-spike method (Table 3; Fig. 4B).

An additional component to these new experiments involved establishing the isotopic homogeneity of the hematite substrate (Table 4; Fig. 4C). We now recog-

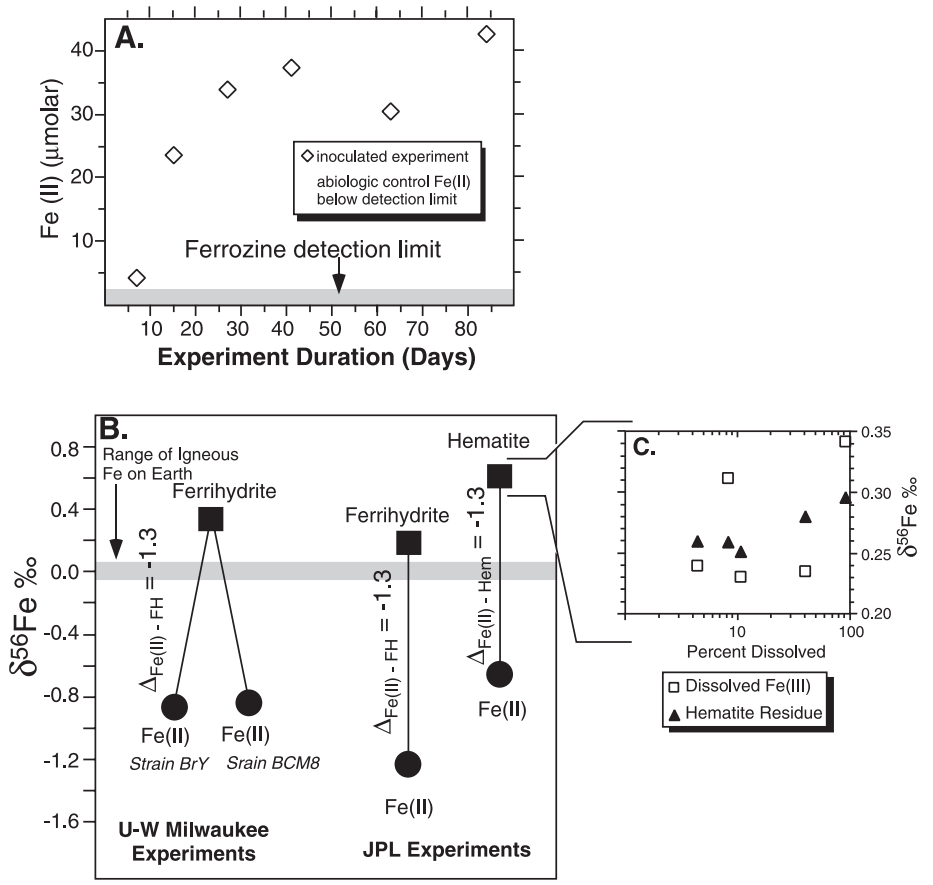

Fig. 4. Iron isotope fractionation by Fe-reducing bacteria. (A) Plot of Fe(II) contents measured in growth media during reductive dissolution of hematite by *S. alga* inoculation, versus days from cell inoculation. Iron contents determined using the *Ferrozine* method. Iron contents analyzed in an abiological control experiment, sampled at the same time as the inoculate experiment, were below detection limits of the *Ferrozine* method (detection limit shown by gray shaded box). (B) Summary of Fe isotope fractionations produced by Fe-reducing bacteria *S. alga*, using different ferric Fe substrates (ferrihydrite and hematite), growth media, and bacterial strains. Particularly notable are the results obtained using hematite as the ferric substrate, in a minimal salts solution media, where abiologic controls had undetectable levels of inorganic Fe dissolution (this study). These results robustly constrain the $\Delta_{Fe(II)-Fe(III)\ SUBSTRATE}$ isotope fractionation for $^{56}Fe/^{54}Fe$ at -1.3 ‰ for Fe(II) produced by Fe-reducing bacteria. Isotopic compositions have been sustained in experiments up to 84 days in length. Summary points represent several dozen analyses conducted by the TIMS double-spike technique and are from Beard et al. (1999) and this study (Table 3). Note that all data have been adjusted for the 0.5 ‰ $\delta^{56}Fe$ bias between TIMS double-spike measurements and MC-ICP-MS analyses (see Skulan et al., 2002). (C) Results of partial dissolution of the hematite substrate used in the *S. alga* experiments (all analyses by MC-ICP-MS method; Table 4). The partial dissolution analyses reveal that the hematite substrate is isotopically homogenous and confirm that no isotopic fractionation occurs during simple dissolution.

nize this as a potentially large problem in any experimental study of Fe isotope fractionation, because synthesis of ferric oxides or oxyhydroxides, in many laboratory conditions, produces isotopically zoned crystals caused by rapid precipitation (Skulan et al., 2002). Partial leaching of such crystals in strong acid, however, does not produce isotopic fractionation during dissolution, allowing measurement of the extent of isotopic zonation in a mineral through step-wise dissolution.

Our new experiments using *S. alga* and hematite substrate demonstrate that the -1.3 ‰ fractionation for $^{56}Fe/^{54}Fe$ during reductive dissolution of ferric oxide is not a result of partial dissolution of an

Table 3
Measured Fe isotope composition of hematite and ferrous Fe produced by reductive dissolution of iron oxide by *S. alga*

Sample	δ^{56}Fe	2 SE	Avg. δ^{56}Fe	1 SD
Stock hematite	0.57	0.15	0.43	0.10
	0.31	0.25		
	0.38	0.16		
	0.50	0.13		
	0.38	0.12		
Reacted hematite 1	0.57	0.13	0.56	0.01
	0.56	0.20		
Reacted hematite 2	0.68	0.20	0.68	0.20
Aqueous Fe(II)[a]	−0.35	0.16	−0.52	0.22
	−0.43	0.12		
	−0.77	0.21		
Aqueous Fe (II)[b]	−0.77	0.12	−0.78	0.13
	−0.70	0.12		
	−0.62	0.16		
	−0.88	0.21		
	−0.94	0.25		

Average $\Delta_{Fe(II)-hematite} = -1.27 \pm 0.14$ ‰

Average $\Delta_{Fe(II)-hematite}$ calculated using the four possible pairs of Fe(II) and reacted hematite averages; error is 1 SD of the four pairs. Iron isotope compositions measured by TIMS using a mixed ^{54}Fe–^{58}Fe double spike (Beard and Johnson, 1999; Johnson and Beard, 1999). Reacted hematite is the isotope composition of hematite following 84 days of incubation in a minimal salts growth media inoculated with *S. alga* cells (1 and 2 refer to separate dissolutions of the reacted hematite). Aqueous Fe(II) is the isotope composition of the ferrous iron produced by the reductive dissolution of hematite by *S. alga* bacteria. No detectable aqueous Fe(II) was produced in abiological control experiments.

The reported Fe isotope compositions have been corrected for a small bias (0.5 ‰) between the TIMS and MC-ICP-MS techniques to allow comparison between the partial dissolution studies (Table 4) conducted on the stock hematite by MC-ICP-MS. Note that this correction has no effect on the measured fractionation factor because all data were collected using the TIMS technique. Ferrous contents in growth media at various times after inoculation are shown in Fig. 4.

[a] Fe(II) analyzed using a combustion method (Beard et al., 1999).

[b] Fe(II) analyzed using a precipitation method (Beard et al., 1999).

isotopically zoned substrate (Tables 3 and 4; Fig. 4). Moreover, the isotopic fractionation is identical to that measured using ferrihydrite as a substrate (Fig. 4B). It is striking that Fe reduction by *S. alga* produces a consistent 1.3 ‰ fractionation between Fe(III) substrate and bacterially reduced Fe using a variety of substrates, growth media, and bacterial strains, and that such fractionations can be sustained for ≥ 84 days.

Exactly how bacteria fractionate Fe isotopes during dissimilatory Fe reduction is not certain. Part of this uncertainty stems from the fact that despite extensive interest in the subject (e.g., Nealson, 1983; Tugel et al., 1986; Lovley, 1991; Nealson and Myers, 1992; Ehrlich, 1996), the mechanism for bacterial Fe reduction is not well understood. Processing of Fe by Fe-reducing bacteria logically might involve a number of steps that could fractionate Fe isotopes. These include dissolution of the Fe(III) substrate, transport of dissolved Fe(III) to the cell, binding of Fe(III) at the site of reduction, and Fe reduction and release of Fe(II) (Fig. 5). The actual site of electron transfer to Fe(III) may be on the outer surface of the cell or at some distance from the cell (Gespard et al., 1998; Nevin and Lovley, 2000; Newmann and Kolter, 2000). Furthermore, electron transfer may involve Fe(III) that is still bound to the mineral surface, or has been solubilized and transported (Forsythe et al., 1998; Doug et al., 2000; Nevin and Lovley, 2000; Newmann and Kolter, 2000).

Because dissolution in and of itself is unlikely to fractionate Fe isotopes (Skulan et al., 2002), the step labeled Δ_1 in Fig. 5 is not likely to fractionate Fe isotopes. Moreover, if aqueous Fe(II) is well complexed in solution, the pathway labeled Δ_3 will not be active, and there will not be an isotopic discrimination. We therefore tentatively conclude that the most likely step that involves Fe isotope fractionation is between Fe(III)–L_1 and Fe(II)–L_2, where L_1 and L_2 are ferric- and ferrous-bound ligands, respectively (Fig. 5). As we will show below, Fe isotope fractionation between hexaquo Fe(III) and Fe(II) complexes produces a +2.7 ‰ *equilibrium* Fe isotope fractionation at room temperature, which is about twice that measured in the *S. alga* experiments; it is tempting to conclude that this disparity represents a "steady-state" *kinetic* isotope fractionation or "vital" effect, but it is also possible that the nature of the ligands L_1 and L_2 is important contributors to the overall Fe isotope fractionation.

Dissolution of hornblende in the presence of organic ligands such as siderophores appears to fractionate Fe by as much as −0.8 ‰ in ^{56}Fe/^{54}Fe (Brantley et al., 2001). Moreover, the magnitude of the Fe isotope fractionation during dissolution in these

Table 4
Fe isotope composition of partial dissolution tests of hematite used in *S. alga* experiment to determine if hematite is isotopically homogenous

Sample	% Hem dissolved	δ^{56}Fe	2 SE	δ^{57}Fe	2 SE	Avg. δ^{56}Fe	1 SD
Dissolved Fe(III)	4.4	0.25	0.06	0.44	0.04	0.24	0.01
		0.23	0.06	0.40	0.04		
Hematite residue	4.4	0.26	0.05	0.39	0.04	0.26	0.05
Dissolved Fe(III)	8.3	0.29	0.04	0.42	0.03	0.31	0.03
		0.33	0.07	0.47	0.04		
Hematite residue	8.3	0.26	0.04	0.39	0.04	0.26	0.04
Dissolved Fe(III)	10.7	0.23	0.07	0.42	0.04	0.23	0.07
Hematite residue	10.7	0.25	0.04	0.41	0.04	0.25	0.04
Dissolved Fe(III)	40.6	0.23	0.05	0.43	0.04	0.23	0.05
Hematite residue	40.6	0.32	0.05	0.38	0.03	0.28	0.05
		0.24	0.07	0.39	0.05		
Dissolved Fe(III)	92.8	0.34	0.07	0.39	0.04	0.34	0.07
Hematite residue	92.8	0.29	0.06	0.38	0.04	0.30	0.01
		0.30	0.07	0.44	0.04		

Iron isotope measurements made using the UW Micromass *IsoProbe*. Percent hematite dissolved was calculated from mass balance based on the total Fe concentration measured in the dissolved fraction using the *Ferrozine* method. 2 SE is two standard errors from the in-run statistics for a single analysis; 1 SD is one standard deviation of two mass spectrometry runs, or the 2 SE if only one analysis was made.

experiments correlates with the binding constant of the chelating agent, where higher binding strength ligands produce larger differences in isotope composition between the aqueous Fe and solid Fe substrate (amphibole). Dissolution by itself is not expected to produce significant isotopic fractionation unless dissolution rates are much slower than solid-state diffusion rates, assuming dissolution occurs smoothly along an advancing front and does not exploit crystal defects or other internal structures. However, if recrystallization or precipitation occurs on mineral surfaces during dissolution, creation of isotopically distinct pools of Fe may occur, which is required by mass balance if dissolved Fe in solution is isotopically light. It may be, for example, that the process of organic complexation is the step that involves isotopic fractionation in our *S. alga* experiments. Despite the uncertainties in the mechanism of isotope fractionation, the data of Brantley et al. (2001) clearly show that Fe complexed with organic ligands is isotopically light as compared to amphibole, which was the ultimate source of the organically complexed Fe. However, macroscopic experiments such as ours, or those of Brantley et al., are not able to assess in detail isotopic fractionations that may exist between multiple ligands or on mineral surfaces, preventing full

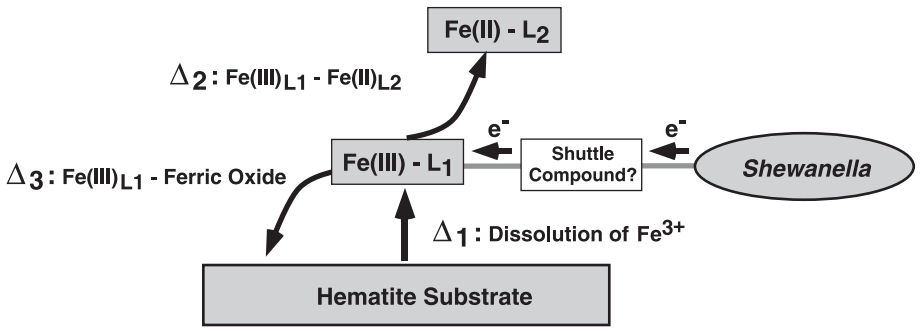

Fig. 5. Possible pathways by which Fe isotopes may be fractionated by *S. alga*. Dissolution (Δ_1) is unlikely to produce isotopic fractionation (Fig. 4C; Skulan et al., 2002), and if Fe(II) is well complexed in solution, precipitation of ferric oxides (Δ_3) is unlikely to be a factor. We consider the most likely step to produce isotopic fractionation to be (Δ_2) reflecting isotopic fractionation between the main exchangeable pools (ligand bound) of Fe.

accounting of all isotopic reservoirs so that the mass balance of the system may be checked. Although we have no resolution to this discussion, it should be clear that future macroscopic experiments must also include studies at a mechanistic level, before we will understand isotopic fractionation during biological processing of Fe.

One study of Fe isotope fractionation during biogenic mineral precipitation has been reported by Mandernack et al. (1999), who note minimal net Fe isotope fractionation during formation of intracellular magnetite by magnetotactic bacteria. Although both aqueous Fe(III) and magnetite were not measured as a function of reaction progress for these experiments, mass balance calculations reported by Mandernack et al. (1999) suggest that any net isotopic fractionation is less than 0.3‰ for $^{56}Fe/^{54}Fe$, which is at the uncertainty limit of the TIMS measurements used in this study. However, it would be premature to conclude that there is no "vital" effect produced by magnetotactic bacteria based on these results because we do not yet know the isotopic fractionations for the steps involved in producing intracellular magnetite. Moreover, we must contrast these results with equilibrium Fe isotope fractionations that may occur between dissolved Fe and magnetite. For example, combining the Fe isotope fractionation factors predicted for magnetite (Polyakov and Mineev, 2000) and hexaquo Fe(III) and Fe(II) (Schauble et al., 2001), the Fe(III)–magnetite and Fe(II)–magnetite fractionations are predicted to be +1.2‰ and −4.4‰ for $^{56}Fe/^{54}Fe$, respectively, at 25 °C. It certainly may be possible that there is indeed a net "vital" effect during production of intracellular magnetite by magnetotactic bacteria, but that this is in the opposite direction of an equilibrium isotope fractionation.

The questions raised by experimental studies of Fe isotope fractionation in biological systems, such as the role of ligands or "vital" effects during dissolution and precipitation of minerals, underscores the need to simultaneously develop a database of equilibrium Fe isotope fractionation factors for geologically relevant minerals and fluids at low temperatures.

4.2. Abiologic Fe isotope fractionation

In our initial work on Fe isotopes (Beard and Johnson, 1999; Beard et al., 1999), we suggested that equilibrium Fe isotope fractionation produced by inorganic processes might be very small. This idea was based on the fact that bulk-earth Fe had a homogenous Fe isotope composition as determined by analysis of a variety of igneous rocks, whereas for samples that formed at low temperature, where a biological influence was likely, $\delta^{56}Fe$ values were strikingly similar to the fractionations measured in our biological experiments. An alternative interpretation is that the large range in $\delta^{56}Fe$ values of rocks and minerals that formed at low temperatures simply reflects mass-dependent Fe isotope fractionation, which would be expected to be the largest in low temperature environments. However, the remarkable constancy of igneous rocks in their Fe isotope composition, relative to their O isotope compositions, which clearly record incorporation of ^{18}O-rich sedimentary components in some cases, poses a problem: are the low-temperature components that are recorded in the moderate- to high-$\delta^{18}O$ values of many continental igneous rocks not seen in their $\delta^{56}Fe$ values, or are anomalous $\delta^{56}Fe$ values of low-temperature rocks and minerals so rare, that it is unlikely that they would ever be recorded in continental igneous rocks?

Understanding the origin of anomalous $\delta^{56}Fe$ values in natural minerals and rocks, as well as the lack of such variations in igneous rocks, requires careful experimental determination of equilibrium Fe isotope fractionation factors between various aqueous species and minerals. As discussed above, such data are also important for interpretation of the results from biological experiments. It is critical that such experiments distinguish between kinetic and equilibrium Fe isotope fractionation, which can be quite difficult at the low temperatures (≤ 200 °C) that characterize near-surface environments. The most rigorous approach to demonstrating attainment of isotopic equilibrium is through isotopic exchange reactions, ideally approached from two sides, and possibly including multiple isotope ratios as tracers, such as that employed by the "three isotope method" (Matsuhisa et al., 1978). In practice, such approaches can only be used at high temperatures (>500 °C), and even at these temperatures, extrapolation of partial exchange results is a common necessity (e.g., Northrop and Clayton, 1966). Despite development of these clever techniques, if the degree of isotope exchange is not large (>80%), the precision of the estimated fractio-

nation factor can be poor because of error multiplication.

In situations where true isotope exchange reactions are not possible because exchange rates are slow (i.e., at low temperatures), synthesis experiments conducted at very slow rates (weeks to months) are used as the best estimate for the equilibrium fractionation factor. Attainment of isotopic equilibrium between aqueous species is generally much easier than between mineral–mineral or mineral–solution pairs, although in the case of experimental systems involving aqueous species, rapid separation may be difficult. Several studies have investigated Fe isotope fractionation in abiologic laboratory experiments, reflecting a variety of kinetic and equilibrium isotope effects (e.g., Anbar et al., 2000; Bullen et al., 2001; Matthews et al., 2001; Johnson et al., 2002; Skulan et al., 2002). We focus first on experiments that bear on aqueous speciation, followed by discussion of mineral–solution isotope fractionations. We conclude with a comparison of experimentally determined Fe isotope fractionation factors that most closely approximate equilibrium fractionation with those predicted from spectroscopic data.

4.2.1. Speciation experiments

Evaluating the magnitude of Fe isotope fractionation in aqueous solutions is challenging because it is difficult to isolate two aqueous Fe species by a method that preserves the equilibrium fractionation factor between them. For example, if the rate of isotopic exchange between the two aqueous species is more rapid than the rate at which the two Fe species are separated, the measured isotopic contrast may be far from that of the equilibrium fractionation factor due to continued isotopic exchange during separation. This effect can be quite dramatic as the mass balance of the system changes during separation (Johnson et al., 2002). Moreover, one must be cognizant of possibly introducing a laboratory fractionation in the separation process that could mask the fractionation factor between the two aqueous species. For example, if the separation procedure is not quantitative, then the measured fractionation factor may represent the fractionation associated with a laboratory separation process, such as precipitation or selective binding of one component, as well as the net fractionation between the two aqueous species.

The first study of Fe isotope fractionation in an abiologic experimental system is that of Anbar et al. (2000), who inferred Fe isotope fractionation between different ferric iron chloro complexes in a free-flowing ion-exchange column. Separation of aqueous Fe chloro complexes was accomplished by loading a solution of ferric iron in 7 M HCl onto a chromatographic column packed with anion-exchange resin, followed by elution of ferric iron using 2 M HCl. In this system, the Fe that was initially loaded onto the column existed primarily as a tetrahedral $[FeCl_4]^-$ complex, a Fe complex that is preferentially bound to anion-exchange resin. In 2 M HCl, Fe occurs predominately as the $[FeCl]^{2+}$ complex with minor, but sub-equal amounts of the $[FeCl_3]^0$ and $[FeCl_2]^+$ complexes (Bjerrum and Lukeš, 1986). Therefore, as 2 M HCl is added, the $[FeCl_4]^-$ is progressively changed to complexes that are less coordinated with Cl, and which have a lower affinity for anion-exchange resin as compared to the $[FeCl_4]^-$ complex. Based on curve fitting of the measured Fe isotope composition with respect to the cumulative proportion of Fe collected, Anbar et al. (2000) concluded that the range of measured Fe isotope compositions could best be interpreted to reflect a 0.1 ‰ equilibrium fractionation in $^{56}Fe/^{54}Fe$ between $[FeCl_4]^-$ and $[FeCl_3]^0$, although attainment of isotopic equilibrium was assumed rather than demonstrated.

In the Anbar et al. (2000) experiment, there are three possible steps that could produce Fe isotope fractionation: a fractionation between different Fe chloro complexes, a fractionation during binding of Fe onto the resin, and a fractionation associated with removal of Fe from the resin. Moreover, if the isotopic exchange rate between different Fe chloro complexes is more rapid than the exchange rate between immobile Fe (resin bound) and mobile Fe (Fe not bound to the resin), the measured fractionation factor would more likely reflect kinetic fractionation that occurred during partial isotopic exchange between different Fe chloro complexes as the Fe species were absorbed and desorbed from the resin.

Isotopic equilibrium can be rigorously demonstrated for experiments using a ^{57}Fe-tracer approach, and we have used this method to investigate the amount of time required for isotopic equilibrium to occur between resin bound and nonresin-bound Fe in anion-exchange resins. The rate of Fe isotope exchange was measured in a batch experiment (Fig. 6A), where anion-exchange

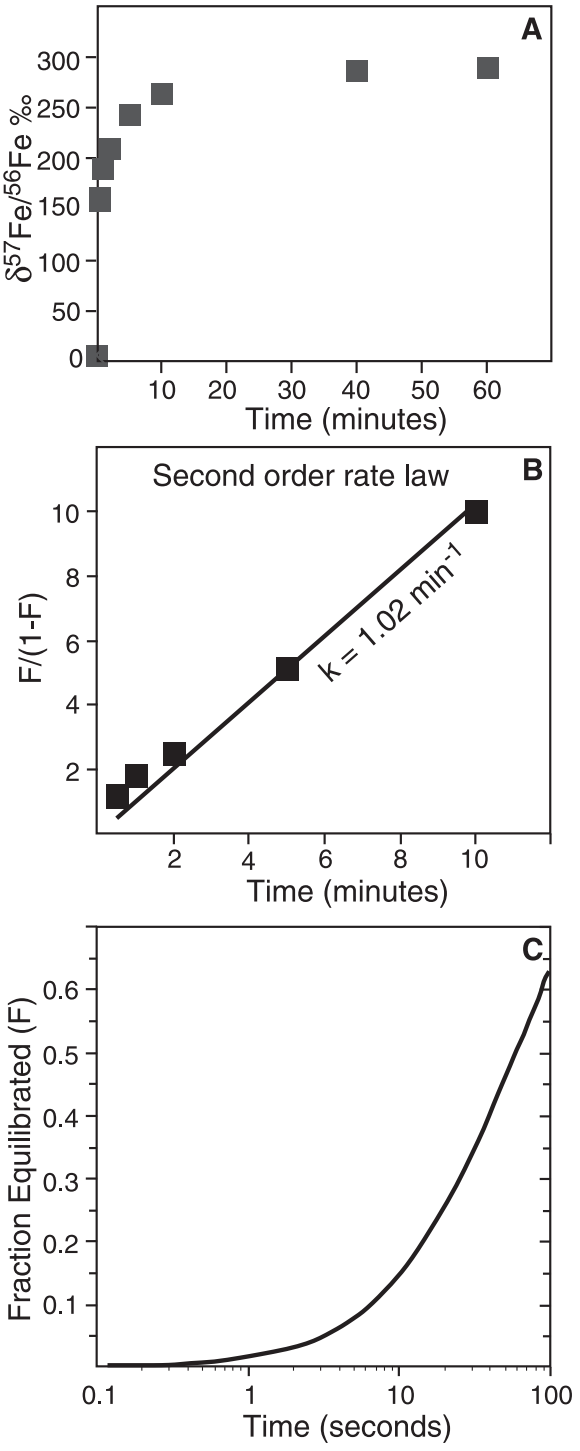

Fig. 6. ^{57}Fe-tracer experiment that evaluates the time required to reach isotopic equilibrium between resin bound Fe and aqueous Fe in 6 M HCl in a "closed" batch system, with shaking between sampling. (A) Plot of the $\delta^{57}Fe/^{56}Fe$ of aqueous Fe in 6M HCl (supernatant) versus the time since a solution of normal Fe isotope composition was added to anion exchange resin (AG 1X4 200–400 mesh) that had been equilibrated with an enriched ^{57}Fe solution (see text for details). (B) Plot of the extent of exchange toward isotopic equilibrium [$F=(\delta-\delta_i)/(\delta_e-\delta_i)$] (Criss, 1999) versus time. The data are best fit by a second-order rate law with a reaction rate of 1.02 min^{-1}. See Johnson et al. (2002) for discussion of rate law formulations. (C) Plot of the percent isotopic equilibration versus time for Fe isotope exchange between resin bound Fe and aqueous Fe in 6M HCl in the experiment of A and B, using a second-order rate law and a reaction rate of 1.02 min^{-1}.

resin that had been loaded with a ^{57}Fe-enriched solution was equilibrated with a solution of Fe in 6 M HCl. Initially, 30 ml of a ^{57}Fe-enriched, 106 ppm 6 M HCl solution ($\delta^{57}Fe/^{56}Fe=+470$ ‰) was mixed with 0.175 g of AG 1X4 200–400 mesh resin, where 32% of the Fe was absorbed after equilibration. The ^{57}Fe-enriched solution was decanted from the resin, with some pore fluid remaining, followed by addition of 5 ml of a 120-ppm Fe 6 M HCl solution of normal Fe isotope composition ($\delta^{57}Fe/^{56}Fe=0$ ‰). The mixture was shaken, which produced a mixed pore fluid + solution $\delta^{57}Fe/^{56}Fe$ value of $\sim +4$ ‰, based on mass balance estimates, immediately after shaking (see Table 5). Successive 100 μl samples were taken over time from the mixture for isotopic analysis. The bottle containing liquid and resin was vigorously shaken during the course of the sampling to ensure that the resin was suspended in the liquid. The $\delta^{57}Fe/^{56}Fe$ values of the liquid increase with increasing time, and by 60 min, complete isotopic equilibration between resin and acid has occurred. The $\delta^{57}Fe/^{56}Fe$ value of the liquid after 60 min was +290.6 ‰ and this value is identical within error to the value measured for Fe extracted from this resin after an additional 4 h of equilibration ($\delta^{57}Fe/^{56}Fe=+291.2$). The Fe concentration of the liquid was measured for each of the time series to determine the extent of net mass transfer between the resin and the liquid. The Fe concentration in the liquid fractions for all the samples is similar (Table 5). Hence, we conclude that during most of the experiment, the total net mass transfer was negligible. However, at the onset of the experiment there was a net mass transfer of iron from the solution to the resin. The initial normal Fe concentration of the solution

Table 5
Fe isotope composition of ^{57}Fe exchange experiment between resin bound Fe and aqueous Fe in 6 M HCl

Sample description	Fe conc. ppm	$\delta^{57}Fe/^{56}Fe$ ‰
Stock ^{57}Fe solution	106.1[a]	470.1
^{57}Fe solution after Equil. with resin	76.6	469.5
Normal Fe stock solution	120.8[a]	−0.2
Initial liquid composition[b]	120.1	4.4
Liquid after 30 s Equil.	102.7	162.2
Liquid after 31 s Equil.	96.1	159.6
Liquid after 1 min Equil.	103	190.7
Liquid after 2 min Equil.	95.7	209.6
Liquid after 5 min Equil	90.9	244.4
Liquid after 10 min Equil	84.8	265.1
Liquid after 40 min Equil.	95.4	287.9
Liquid after 60 min Equil	98.5	290.6
Resin after 5 h Equil[c]		291.2

Batch experiment with continued shaking, except during sampling of supernatant. The Fe isotope compositions and Fe concentrations of these enriched ^{57}Fe experiments were measured by MC-ICP-MS using a cyclonic spray chamber to allow for rapid wash out of samples, which is critical for samples that have dramatically different Fe isotope compositions. Using this method, the measured $^{57}Fe/^{56}Fe$ ratios are precise to ±0.5‰ based on eight replicate analyses of UW HPS Fe. The reported Fe isotope compositions are relative to UW HPS Fe. Fe concentrations were determined by comparison of total measured ion intensities to a standard curve constructed from Fe standard of various Fe concentrations. The measured Fe concentration of the sample used for isotope analysis are precise to ±3–5% (based on scatter of the constructed standard curve), but because of weighing errors in the dilution of these samples for isotope analysis, the actual precision of the reported Fe concentration is ±10%.

[a] Concentration is known from gravimetry.

[b] The concentration and isotopic composition of the initial liquid are greater than the isotopic composition of the normal Fe stock solution because of the ^{57}Fe-rich pore fluid in the resin. The concentration and isotope composition of this liquid were calculated from mass balance assuming that resin has a 30% pore volume and that the ^{57}Fe-rich pore fluid had the same Fe concentration and isotope composition that was measured for the ^{57}Fe stock solution after equilibration with the resin.

[c] The isotope composition of Fe bound to the resin after 5 h of equilibration was determined by filtering the solution from the resin and then stripping the resin bound Fe using 0.5 M HCl. A total of 993 μg of Fe was collected from the resin.

was 120 ppm and after addition of this solution to the ^{57}Fe loaded resin, the Fe concentration dropped to 103 ppm Fe.

The data for this 6 M HCl ^{57}Fe-tracer experiment are best fit by a second-order rate law with a reaction rate of 1.02 min^{-1} (Fig. 6B), indicating that, for example, in 1 min, there will be ~50% isotopic exchange between resin-bound Fe and aqueous Fe in a 6 M HCl solution (Fig. 6C). This reaction rate does not include data for the samples taken at 40 and 60 min because these solutions are so close to the equilibrium isotopic value that small errors (±0.5‰) in the measured $\delta^{57}Fe/^{56}Fe$ value result in large errors in the rate constant determination. This error magnification is a result of the fact that for a second-order rate law, the rate constant is linearly related to $F/(1-F)$ where F is the equilibration proportion (Johnson et al., 2002). We consider that the reaction rate determined using the experimental set up to be a maximum value because small amounts of resin (0.5–1.0 mg) remained entrained in the liquid after shaking stopped, particularly for early samples. Any resin remaining in the 100 μl aliquots was removed by centrifuging for 5 min, which provided additional time for continued exchange. This additional equilibration time makes it appear that the resin and liquid had moved closer to the equilibrium value than it actually had when the liquid aliquot was taken. Moreover, there was some mass transfer of Fe from the liquid to the resin when the normal Fe solution was initially added to the ^{57}Fe loaded resin. The addition of Fe with a normal Fe isotope composition to the resin implies that the initial $\delta^{57}Fe/^{56}Fe$ of the resin was lower than assumed. The lowering of the initial $\delta^{57}Fe/^{56}Fe$ of the resin also makes it appear that the samples are closer to equilibrium than if the resin had the high $\delta^{57}Fe/^{56}Fe$ that we assumed it to have.

The purpose of these ^{57}Fe-tracer experiments is to highlight the fact that attainment of isotopic equilibrium in ion-exchange systems is not instantaneous, and to urge caution when interpreting the results of measured isotope compositions in the absence of parallel isotopic tracer experiments. Use of anion-exchange resin to evaluate equilibrium fractionation between aqueous Fe species requires that the isotopic exchange rate between the aqueous species be slower than that between the aqueous Fe and resin-bound Fe. In contrast, if the isotopic exchange rate between aqueous species is more rapid than that between the resin bound and aqueous Fe, then the isotopic exchange kinetics between the various aqueous species, and between the resin bound and aqueous species, must be known to evaluate how the isotopic re-equilibration between aqueous species will affect

the measured isotopic compositions of the solution Fe.

Comparison of the results of our kinetic exchange experiment with the experiments conducted by Anbar et al. (2000) is difficult because the experimental designs are significantly different. The ^{57}Fe-tracer exchange experiments were batch experiments, and those of Anbar et al. (2000) were dynamic experiments using free-flowing HCl in a column with changes from 7 to 2 M HCl. It seems likely that in this dynamic experiment, numerous isotope exchange reactions take place as the initial $[FeCl_4]^-$ complex in 7 M HCl is absorbed onto the resin, followed by conversion to various Fe chloro complexes as 2 M HCl was eluted through the column. Because the isotopic exchange rate between various Fe chloro complexes is unknown, it is difficult to predict the effects that partial or complete isotopic re-equilibration between the various Fe chloro complexes would have on the inferred fractionation between $[FeCl_4]^-$ and $[FeCl_3]^0$.

Matthews et al. (2001) investigated Fe isotope fractionation between Fe(II) complexed with an organic molecule (2,2′ bipyridine) and $[FeCl_4]^-$, using anion-exchange resin to separate the Fe species. Because measured isotopic fractionation correlated with the mole fraction of Fe(II), Matthews et al. interpreted the isotopic variations to record kinetic isotope effects, reflecting the combined influences of isotopic fractionation during ion-exchange separation and dissociation of $[Fe^{II}(bipy)_3]^{2+}$ in 6 M HCl.

It appears that ion-exchange resin, although a convenient method for separation of aqueous species, may not be the best method for separation of aqueous complexes if the goal is to measure equilibrium isotope fractionation because isotopic equilibration between resin-bound species and aqueous complexes may be significantly slower than assumed, and complex kinetic reactions may be more important than previously realized. The relatively slow nature of ion-exchange equilibration was noted in many of the initial works that discussed anion resin exchange several decades ago; equilibrium absorbability studies often required equilibration times of 1 day or more (e.g., Kraus and Nelson, 1956).

Equilibrium isotopic fractionation for $^{56}Fe/^{54}Fe$ between $[Fe^{III}(H_2O)_6]^{3+}$ and $[Fe^{II}(H_2O)_6]^{2+}$ has been measured using a rapid (≤ 1 s) carbonate precipitation method to separate ferric and ferrous species, producing $\Delta_{Fe(III)-Fe(II)} = +2.75‰$ at 22 °C (Johnson et al., 2002). Parallel ^{57}Fe-tracer experiments indicate that the data may be fit to a second-order rate law, with a reaction rate of 0.18 s^{-1}, indicating that ~95% exchange occurs within 3 min. Measurement of the exchange kinetics also allowed minor corrections to be made to $\Delta_{Fe(III)-Fe(II)}$ due to small amounts of partial re-exchange during species separation, although this correction was $<0.10‰$ (Johnson et al., 2002). These results provide clear indication that abiologic equilibrium Fe isotope fractionation occurs between aqueous ferric and ferrous Fe in solutions that closely approximate those found in natural, near-surface environments. That the isotopic fractionations reflect equilibrium isotope effects between aqueous species is well constrained by the ^{57}Fe-tracer experiments, and the fact that the experiment only involved aqueous species in the isotope equilibration step.

The experiments conducted by Bullen et al. (2001) have been interpreted to reflect isotopic fractionation as a function of speciation. In these experiments, the δ^{56}Fe value of ferrihydrite produced by precipitation was greater than that of the mixed aqueous Fe(II) and (III) solution. Because the precipitate was isotopically heavy as compared to the reactant, and steady-state Fe concentration was reached in the flow-through reactor, Bullen et al. (2001) argued that the isotopic difference between ferrihydrite and aqueous Fe must represent the equilibrium fractionation factor between aqueous ferrous iron species. However, it is uncertain if the variations in measured isotope compositions reflect isotopic fractionation between ferrihydrite and aqueous Fe, between various aqueous Fe species, or a combination of both. Moreover, it is difficult to assess if the isotopic fractionations reflect equilibrium or kinetic isotope effects. The experiments by Bullen et al. (2001) reflect a dynamic open system, where the aqueous ferric to ferrous concentration was held at steady-state condition. Although over extremely long time scales, a steady-state system might approach apparent chemical equilibrium, such dynamic flux systems cannot be proven to be in isotopic equilibrium. Moreover, in this experiment, there are two steps that may produce Fe isotope fractionation, oxidation of the aqueous ferrous iron to aqueous ferric iron, and precipitation of ferrihydrite from ferric iron. A kinetic isotope fractionation associated with rapid

precipitation of ferrihydrite could in part mask the true equilibrium Fe isotope fractionation between aqueous ferrous and ferric iron, and this seems to occur over short (hours to days) laboratory time scale (below; Skulan et al., 2002). In addition, because ferrihydrite precipitation rates are controlled by the composition of the fluid (Cornell and Schwertmann, 1996), the apparent control that pH and $[Fe(HCO_3)]^+$ appear to have on the measured fractionation factor may represent changes in ferrihydrite precipitation rate rather than strict controls on the equilibrium fractionation factor between aqueous Fe species.

4.2.2. Aqueous Fe—mineral fractionation

The experimental hurdles in determining equilibrium isotopic fractionation at low temperatures between fluids and minerals are high. Diffusion rates in solids at low temperature are much too slow for true isotopic exchange reactions to occur between mineral and fluid over reasonable time scales, necessitating use of a synthesis approach (e.g., slow solid precipitation from a solution). We have investigated Fe isotope fractionation between hematite and aqueous Fe(III) at a variety of hematite precipitation rates, via an acid hydrolysis reaction (Skulan et al., 2002). This method is similar to the low temperature hematite–water O isotope fraction studies conducted by Bao and Koch (1999), whereby an aqueous ferric iron solution prepared from an $Fe(NO_3)_3$ salt precipitates hematite by forced acid hydrolysis (Schwertmann and Cornell, 1991). In this set of experiments, a series of ferric solutions, prepared from ferric nitrate salts, were sealed into glass ampules and placed in a 98 °C oven. Samples were taken from the oven at different times, ranging from 1 h to 32 days. Hematite and the aqueous Fe were separated by centrifuge and the hematite and aqueous Fe aliquots were analyzed for their Fe isotope compositions. The difference in Fe isotope composition between hematite and aqueous Fe(III) ($\Delta_{Fe(III)-hematite}$) is a strong function of the time that the two phases were in contact with one another (Fig. 7A). Initially, $\Delta_{Fe(III)-hematite}$ rapidly increases to large values, and with time $\Delta_{Fe(III)-hematite}$ becomes progressively smaller. Aqueous Fe(III) contents initially decrease in the first day of the experiment (aqueous Fe concentration is ~ 0.2% of the initial concentration after 12 h), reflecting rapid precipitation of hematite. Following the initial rapid hematite precipitation stage, aqueous Fe concentration remains constant, reflecting the fact that there is no net mass transfer of Fe between hematite and aqueous Fe. However, during this steady-state Fe concentration period, iron is exchanged between hematite and the fluid by dissolution and reprecipitation as determined by ^{57}Fe exchange studies between hematite and aqueous Fe(III), as well as by SEM images that reveal dissolution pits (Skulan et al., 2002).

During the initial stages of this reaction (12 h), at a rapid hematite precipitation rate, the Fe isotope fractionation between hematite and Fe(III) can be modeled as a Rayleigh distillation process using $\Delta_{Fe(III)-hematite} = +1.3$ ‰ (Fig. 7B). The hematite produced by this rapid precipitation process is isotopically zoned as determined by step-wise leaching of hematite after 98% precipitation, which shows that the crystals are strongly zoned in their Fe isotope compositions (Fig. 7C). This initial isotopic fractionation is inferred to have originated from kinetic effects rather than by an equilibrium crystal fractionation process because the measured Fe isotope fractionation between hematite and aqueous Fe(III) is a strong function of time (Fig. 7A).

Based on a series of long-term experiments (up to 203 days) that involved a variety of hematite synthesis rates and initial conditions, we suggest that the equilibrium $\Delta_{Fe(III)-hematite}$ is very close to zero (Skulan et al., 2002). Extrapolation of experiments that involved average hematite precipitation rates between 0.02 and 0.15 μg Fe/day to zero precipitation rate provides an estimate of the equilibrium $\Delta_{Fe(III)-hematite}$ fractionation factor of -0.10 ± 0.20 ‰ at 98 °C (Skulan et al., 2002). These results highlight the importance of distinguishing between kinetic and equilibrium isotope fractionation in experimental studies, and suggest that the Fe isotope composition of hematite may faithfully record the isotopic composition of Fe(III) in dilute aqueous solutions.

4.2.3. Theoretical predictions

Several workers have predicted significant equilibrium Fe isotope fractionations based on spectroscopic data. Polyakov and Mineev (2000) modeled ^{57}Fe-Mössbauer data to predict Fe isotope fractionation between various minerals. Schauble et al. (2001) used infrared, Raman, and inelastic neutron scattering measurements of vibrational frequencies of Fe salts to predict Fe isotope fractionations for coexisting aque-

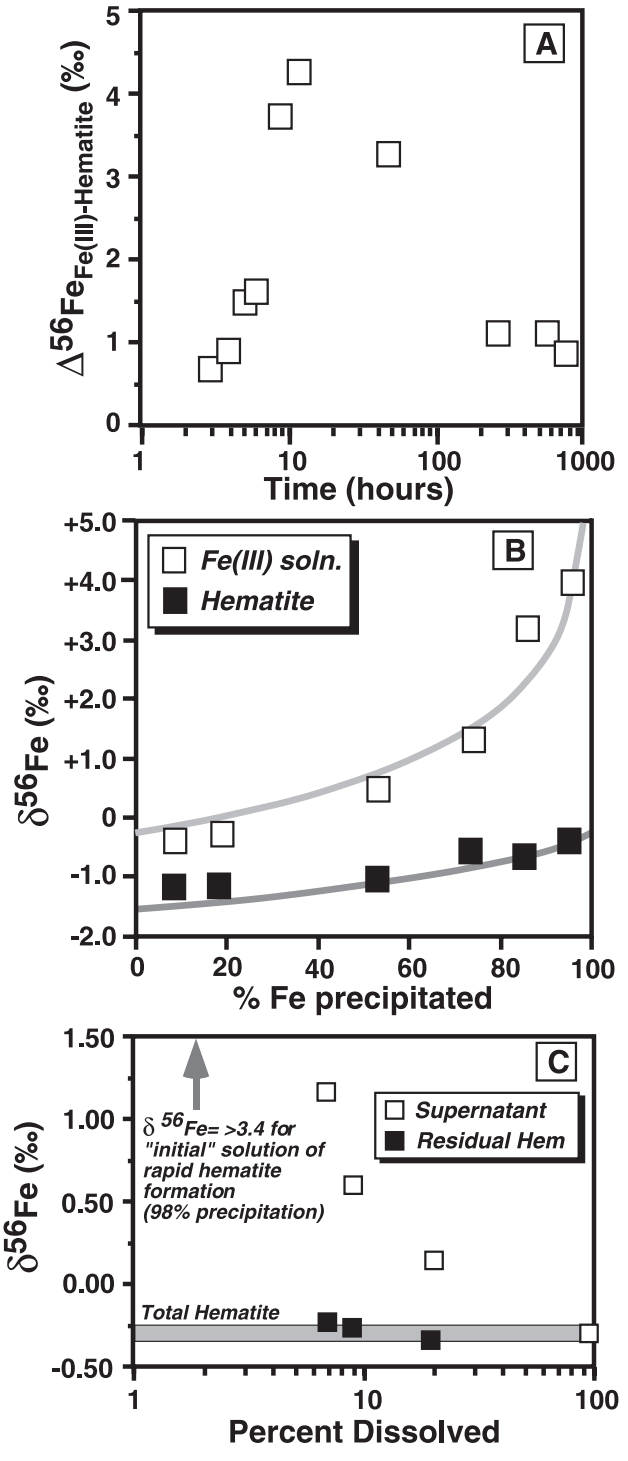
A
$\Delta^{56}Fe_{Fe(III)\text{-}Hematite}$ (‰)
Time (hours)
B
Fe(III) soln.
Hematite
$\delta^{56}Fe$ (‰)
% Fe precipitated
C
Supernatant
Residual Hem
$\delta^{56}Fe$ (‰)
$\delta^{56}Fe$= >3.4 for "initial" solution of rapid hematite formation (98% precipitation)
Total Hematite
Percent Dissolved

ous Fe species, applying a modified Urey–Bradley force field model. Significantly, Schauble et al. (2001) predicted Fe isotope fractionations between Fe-cyanide compounds and metal that are similar to those predicted by Polyakov and Mineev (2000), despite their markedly different approaches. Moreover, the approaches taken by Polyakov and Mineev (2000) and Schauble et al. (2001) have proven successful for calculating oxygen isotope fractionations that match those measured in several experimental systems.

Over the range of temperatures that are pertinent to life and near-surface environments (~ 0 to 200 °C), fractionations in $^{56}Fe/^{54}Fe$ ratios calculated from spectroscopic data suggest isotopic variations up to 6‰ between coexisting aqueous Fe species (Schauble et al., 2001; Fig. 8A). Significant effects by speciation are predicted, including substitution of Cl^- into ferric hexaquo complexes, as well as contrasts in tetrahedral and octahedral Fe chloro complexes. These effects have significant implications for understanding the origin of Fe isotope variations in natural fluids, given the importance of Cl^- in many geological and hydrothermal systems. We may directly compare the predicted isotopic fractionation between $[Fe^{III}(H_2O)_6]^{3+}$ and $[Fe^{II}(H_2O)_6]^{2+}$ with those measured by Johnson et al. (2002), and it can be seen that the predicted fractionation, although correct in sign, is approximately twice that measured by experiment (Fig. 8A). Although some of the discrepancy can be accounted for in the ~ 1‰ errors in the calculated β factors for Fe(III) and Fe(II), as well as the possibility that small amounts (≤ 10%) ferric chloro complexes existed in some of the experimental solutions, there remains at least a 1‰ difference between experiment and prediction.

Combining Fe isotope fractionation factors of Polyakov and Mineev (2000; converted to $^{56}Fe/^{54}Fe$) and Schauble et al. (2001), we can predict mineral–solution Fe isotope fractionation factors (Fig. 8B). Large isotopic fractionations, up to 7‰, are predicted between $[Fe^{III}(H_2O)_6]^{3+}$ and the ferric hydroxides, and smaller, but still significant, isotopic fractionations are predicted between $[Fe^{II}(H_2O)_6]^{2+}$ and siderite (Fig. 8B). The large predicted fractionation between Fe(III) and Fe(II) produces two widely different mineral–solution fractionation curves for magnetite, where relatively small isotopic fractionations are predicted between $[Fe^{III}(H_2O)_6]^{3+}$ and magnetite, but large negative fractionations are predicted for $[Fe^{II}(H_2O)_6]^{2+}$–magnetite. Such large ranges in fluid–mineral fractionations may pose difficulties in calculating the Fe isotope compositions of ancient fluids from measurements of rocks and minerals.

As noted above, in the case of $[Fe^{III}(H_2O)_6]^{3+}$–hematite fractionation, Skulan et al. (2002) estimate this to be −0.10‰ at 98 °C based on experimental determinations. This experimental measurement is far less than the +2.8‰ fractionation that is predicted by the Polyakov and Mineev (2000) and Schauble et al. (2001) datasets (Fig. 8B). Although the kinetic Fe(III)–hematite fractionation of +1.3‰ we measure for rapid precipitation lies somewhat closer to the predicted equilibrium value, this has little relevance to evaluating the predicted isotope fractionations because non-equilibrium isotope fractionation dominates during rapid precipitation (see above). The discrepancy between predicted and experimentally determined Fe(III)–hematite fractionation cannot be reconciled within the uncertainty of the individual β factors calculated by Polyakov and Mineev (2000) and Schauble et al. (2001), which are ~ 1‰ at 100 °C for Fe(III) and hematite.

Although in some cases, the theoretical calculations of Polyakov and Mineev (2000) and Schauble et al. (2001) may be, to a first approximation, suitable for predicting the sign of Fe isotope fractionation in

Fig. 7. (A) Plot of $\Delta^{56}Fe_{Fe(III)-hematite}$ versus the time that aqueous Fe and hematite were allowed to equilibrate. The difference in Fe isotope composition between Fe(III) and hematite increases for the first 12 h and then decreases with time. During the initial 12 h, hematite is precipitating from the fluid and this isotope fractionation can be modeled as a Rayleigh distillation with a fractionation factor of +1.3‰ (see B). After 12 h, the Fe concentration in the solution remains constant, therefore, there is no net mass transfer of Fe between hematite and solution. However, Fe isotope exchange continues and the fractionation factor between hematite and aqueous Fe becomes smaller. (B) Plot of the $\delta^{56}Fe$ value of hematite and aqueous Fe(III) versus the percent Fe precipitated as hematite for the first 12 h of the data shown in A. The measured Fe isotope compositions of hematite and aqueous Fe(III) are fit using a Rayleigh distillation curve and a fractionation factor of +1.3‰ between Fe(III) and hematite (see text for discussion). (C) Partial dissolution of hematite formed from 98% precipitation of an Fe(III) solution, as in B, using 6 M HCl. Hematite produced by rapid (~ 12 h) acid hydrolysis of aqueous Fe(III) is isotopically zoned, where the rims have very high $\delta^{56}Fe$ values. Figure modified from Skulan et al., 2002.

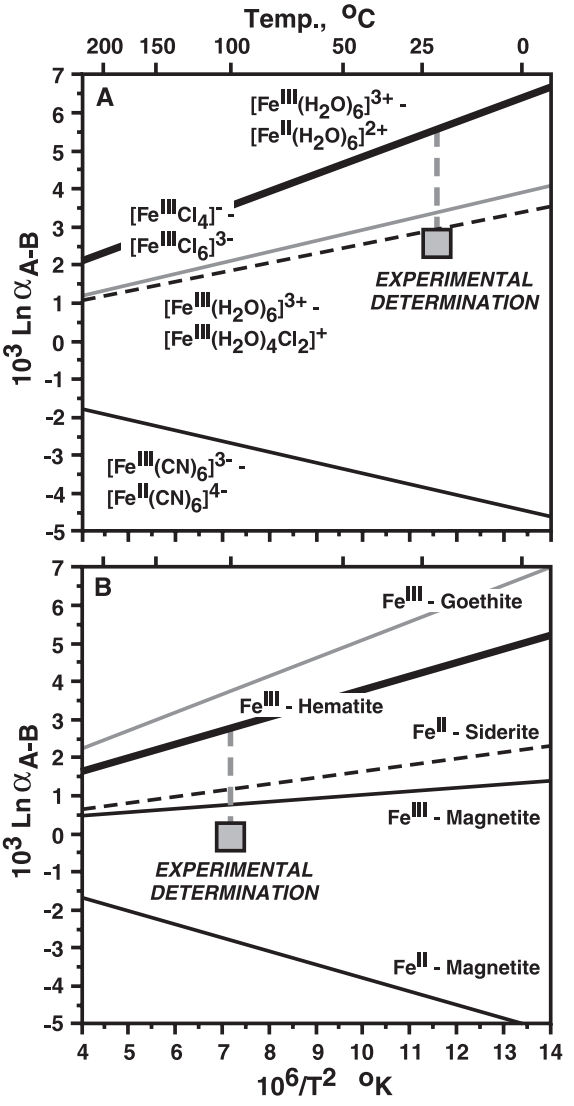

Fig. 8. Comparison of Fe isotope fractionation factors predicted by Polyakov and Mineev (2000) and Schauble et al. (2001) with those determined by experiments. (A) Equilibrium fractionation factors between aqueous ferrous and ferric solutions, as calculated by Schauble et al. (2001), compared to an experimental determination of the equilibrium fractionation factor between Fe(II) and Fe(III) measured by Johnson et al. (2002), showing significant disagreement between calculated and measured values. (B) Equilibrium fractionation factors between aqueous iron solutions and iron oxide, oxyhydroxides, and carbonates, as calculated by Polyakov and Mineev (2000) and Schauble et al. (2001). Experimental determination shown for the equilibrium fractionation factor between Fe(III) and hematite (Skulan et al., 2002), which is markedly different than that calculated using predicted fractionations.

fluids and minerals, initial experimental results indicate that a comprehensive experimental program is needed before Fe isotope variations in natural samples may be understood. Given the relatively restricted range in Fe isotope compositions that have been measured so far, the several per mil discrepancies between experiment and prediction must be resolved.

5. Fe isotope variations in nature

The usefulness of a new isotope system is dependent, of course, on finding measurable variations in natural rocks that record geologically meaningful processes, and initial results clearly demonstrated this to be the case for Fe (Bullen and McMahon, 1998; Beard and Johnson, 1999). Below we summarize the published Fe isotope data that are currently available for natural samples, in addition to a rapidly increasing database from our own laboratory, which document a relatively wide range in Fe isotope compositions for sedimentary rocks and fluids, from the Archean to the present.

5.1. Modern and recent environments

Fig. 9 summarizes the data that are available to us for modern or recent environments, including, hydrothermal spring deposits and waters from New Zealand, Fe–Mn nodules and crusts, as well as data from Archean and Proterozoic Banded Iron Formations (BIFs). Fascinating new Fe isotope data for very slow-growing (1.6 mm/million years; O'Nions et al., 1998) Fe–Mn crusts in the North Atlantic have been presented by Zhu et al. (2000), who demonstrate temporal changes in Fe isotope compositions in the last 6 my; the largest changes occur over the last 2 my, where $^{57}Fe/^{54}Fe$ ratios change by ~ 9 $\delta^{57}Fe$ units (or ~ 0.6‰ in $\delta^{56}Fe$ values; Fig. 9). Because Fe isotope variations are correlated with Pb isotope compositions, Zhu et al. (2000) discount biological processes as the agent responsible for producing the isotopic fractionations, and instead propose that the range reflects isotopic variability in the continental sources of Fe fluxes to the oceans. Given the remarkable Fe isotope homogeneity of terrestrial igneous rocks discussed above ($\delta^{56}Fe = 0.00 \pm 0.05$‰;

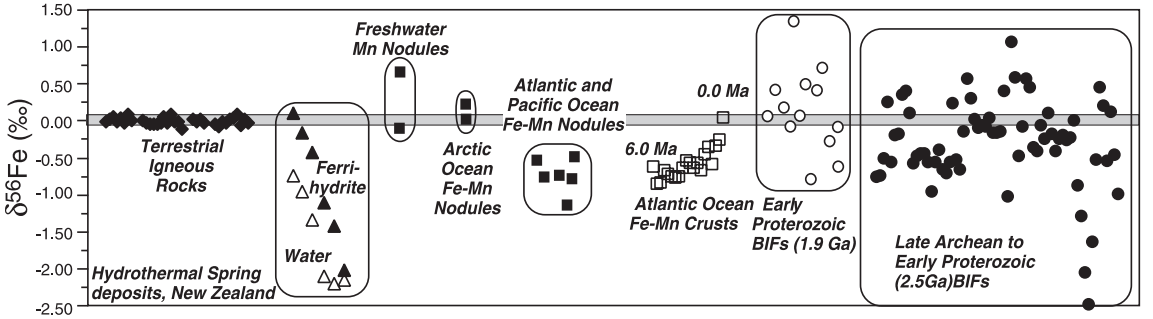

Fig. 9. Summary of Fe isotope data on natural samples. All values are relative to igneous Fe (gray band ± 0.05 ‰); interlaboratory differences are corrected to a $\delta^{56}Fe_{Igneous\ Fe}$ value by setting the $\delta^{56}Fe_{Igneous\ Fe}$ value of IRMM-014 to −0.09 ‰, as measured at the University of Wisconsin-Madison. Data from freshwater, Arctic, Atlantic, and Pacific Fe–Mn nodules are from Beard and Johnson (1999) and Beard et al. (1999). The New Zealand hydrothermal deposit data are from Bullen et al. (2001), illustrating the difference between ferrihydrite and hydrothermal spring waters (note Bullen et al. report Fe isotope compositions relative to an igneous rock, but have not analyzed IRMM-014; these data are plotted as the measured values). Data from Atlantic Ocean Fe–Mn crusts from Zhu et al. (2000), illustrating temporal trend from 6.0 to 0.0 Ma noted by these authors; $^{57}Fe/^{54}Fe$ ratios reported by Zhu et al. (2000) have been converted to equivalent $\delta^{56}Fe$ values by assuming $\delta^{56}Fe = 0.067 * \varepsilon^{57}Fe$, in addition to the offset between IRMM-014 and average igneous Fe. Data for Early Proterozoic Banded Iron Formations (BIF) from the 1.9-Ga sequences in the Lake Superior region, and from Beard and Johnson (1999) and B. Beard and C. Johnson, unpublished data. Data for Late Archean to Early Proterozoic BIFs from the 2.5-Ga Kuruman and Griquatown Iron Formation (South Africa) and 2.5-Ga Dales Gorge member of the Brockman Iron Formation (Hamersley Group, NW Australia); Johnson et al., 2003, and C. Johnson, B. Beard, K. Klein, and N. Buekes, unpublished data. All UW TIMS double-spike data (Fe–Mn nodules and Proterozoic BIF) have been corrected for the 0.5 ‰ offset between the TIMS and MC-ICP-MS measurements.

Table 2), we consider significant Fe isotope variations in continental input to the oceans to be unlikely. Although mixing between water masses was discounted by Zhu et al. (2000), other studies of similar Fe–Mn crusts have interpreted Pb isotope variations to largely reflect such mixing (e.g., Abouchami et al., 1999). It is important to note that the Fe–Mn *crusts* studied by Zhu et al. have very slow growth rates (1.6 mm/million years; O'Nions et al., 1998), and we agree that they are unlikely to have had a *direct* biological component to their precipitation; this contrasts with the Fe–Mn nodules studied by Beard and Johnson (1999), which reflect much higher growth rates (30–300 mm/million years) that likely reflect remobilization of ocean sediment Fe by bacteria at the sediment–water interface (e.g., Finney et al., 1984; Dymond et al., 1984). Clearly, a major effort in Fe isotope studies of seawater, including assessment of any isotopic fractionations that may accompany uptake by phytoplankton (Hudson and Morel, 1989, 1990; Takeda and Obata, 1995; Maranger et al., 1998) or which may exist between various Fe species (Hudson et al., 1992; Gledhill and van den Berg, 1995; Millero et al., 1995; van den Berg, 1995), needs to be pursued before we can understand the processes that control the Fe isotope compositions of the oceans. A major analytical challenge to such an effort will be the very low Fe concentrations in modern seawater.

5.2. Ancient environments

Banded Iron Formations have long played a central role in discussions on the oxygen levels of the Archean and Early Proterozoic atmosphere and the implications for the evolution of life, including the well-known suggestion by Preston Cloud that BIFs reflect weathering and river transport of ferrous Fe, requiring a low oxygen atmosphere, followed by precipitation under locally elevated O_2 contents generated by photosynthesis (Cloud, 1965). BIFs are found on every continent, and significant deposits are found in strata of Early Archean (3.8 Ga) to Late Proterozoic (0.6 Ga) age (see landmark papers and reviews by James, 1954, 1983; Gross, 1965; Trendall, 1968, 1983; Klein and Beukes, 1992; Isley, 1995, for example). The importance of studying BIFs lies not only in evaluating the possible role of organisms in their genesis (e.g., Nealson and Myers, 1990; Widdel et al., 1993; Brown et al., 1995), but also in contrast-

ing the geochemical cycling of Fe in the pre- and post-oxygenated Earth.

Our initial work included only a few Fe isotope analyses of Proterozoic BIFs from the Lake Superior region (Beard and Johnson, 1999). In Fig. 10, we illustrate the Fe isotope variations that are typical of a rapidly developing database on ultra-high-precision Fe isotope analyses of BIFs from the well-known Hamersley Basin, NW Australia (e.g., Trendall and Blockley, 1970; Trendall, 1983), as well as the iron

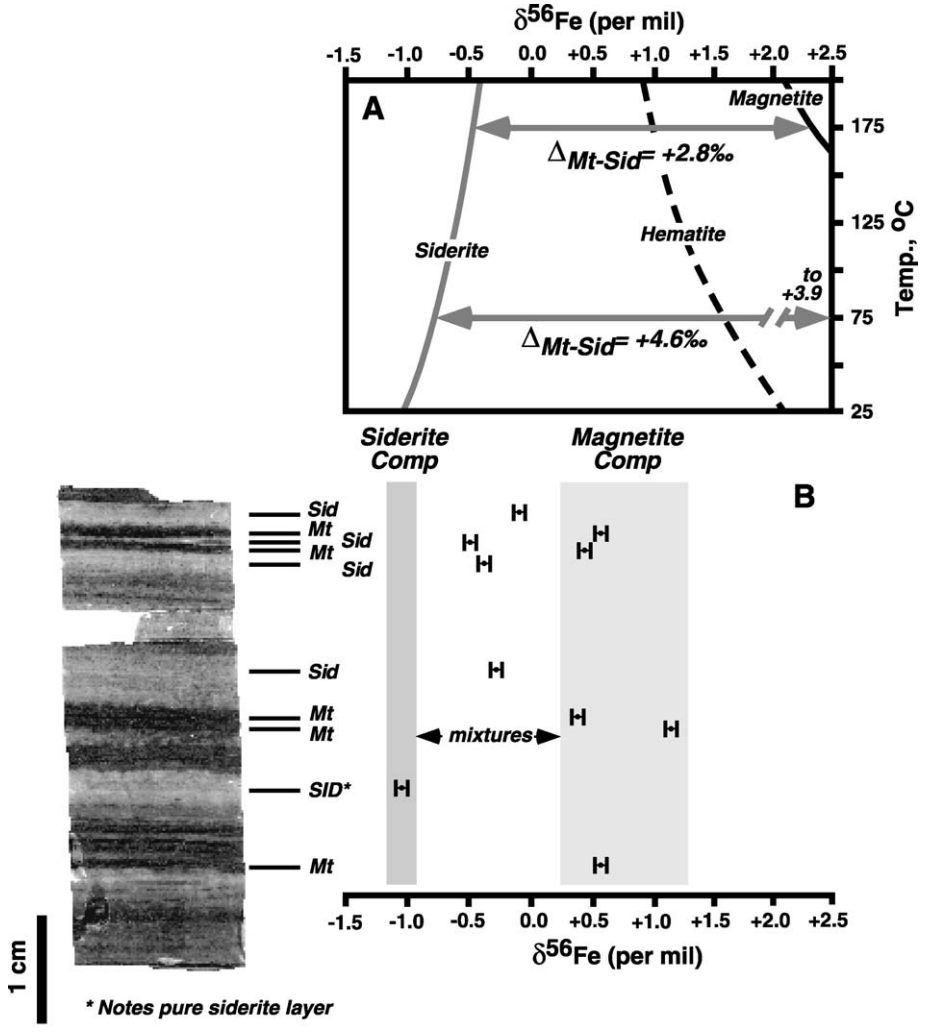

Fig. 10. Comparison of measured Fe isotope compositions in BIFs with those predicted by Polyakov and Mineev (2000). (A) Predicted δ^{56}Fe values of magnetite, hematite, and siderite, as calculated from β factors (adjusted to ^{56}Fe/^{54}Fe ratios) of Polyakov and Mineev (2000). Absolute δ^{56}Fe values calculated assuming δ^{56}Fe of Fe metal (α-Fe) is zero. Calculated δ^{56}Fe values for ankerite plot off scale to the left, where δ^{56}Fe varies from -1.5‰ to -3.0‰ over the temperature range shown. (B) Detailed Fe isotope variations in a section of the 2.5-Ga Kuruman Iron Formation (South Africa), showing isotopic variations between Fe-carbonate and magnetite-rich layers. Generally, the layers reflect mixtures of multiple minerals, where high δ^{56}Fe magnetite is a contaminant to low δ^{56}Fe Fe-carbonate layers; ankerite rich layers have the lowest δ^{56}Fe values (Johnson et al., 2003). The relative orders of decreasing δ^{56}Fe values of magnetite>siderite>ankerite measured in the Kuruman samples are the same as that predicted by Polyakov and Mineev (2000), although much small in magnitude than that predicted for temperature ≤ 170 °C, the maximum metamorphic/diagenetic temperature of the samples (Miyano and Beukes, 1984). Sid = siderite, Mt = magnetite, and Ank = ankerite.

formations of the Transvaal Supergroup, S. Africa (e.g., Beukes, 1983; Beukes et al., 1990), both of which are Late Archean to Early Proterozoic in age (2.5 Ga). Overall, the range in δ^{56}Fe values measured for Late Archean to Early Proterozoic BIFs is from −2.5‰ to +1.5‰, spanning virtually the entire range yet measured on Earth (Fig. 9). Detailed study of the Kuruman Iron Formation in South Africa, for example, indicates that δ^{56}Fe values are generally correlated with mineralogy, decreasing in value in the order magnetite>siderite>ankerite (Fig. 10B; Johnson et al., 2003). δ^{56}Fe values for hematite are variable, but generally scatter about zero (Johnson et al., 2003).

The significant Fe isotope variations preserved in ancient sedimentary rocks immediately raises the question, is this an effect of biology or inorganic processes, or both? One possibility is that the differences in δ^{56}Fe values calculated for pure siderite or ankerite and magnetite in a half-dozen BIF samples from various localities might be explained solely by inorganic equilibrium isotope fractionation. In the South African BIF samples studied so far, magnetite and Fe carbonates commonly appear to be diagenetic in origin (Klein and Beukes, 1989; Beukes et al., 1990; Beukes and Klein, 1990), and it is possible that they formed in Fe isotope equilibrium through diagenetic reactions between Fe(II), carbonate, and primary hematite (Johnson et al., 2003). Assuming that magnetite and siderite formed in isotopic equilibrium, and applying the calculations of Polyakov and Mineev (2000) (Fig. 10A), the measured differences in δ^{56}Fe values suggest temperatures on the order of 300–400 °C, which is significantly higher than the burial diagenesis temperatures (<170 °C) that have been estimated for the Kuruman and Griquatown Iron Formations (Miyano and Beukes, 1984). If the Fe isotope fractionations between siderite and magnetite are solely a result of abiologic isotopic fractionation, are the calculations by Polyakov and Mineev correct in sign but incorrect in magnitude (Fig. 10A), or were kinetic isotope fractionations responsible for the discrepancy? Do the low δ^{56}Fe values of siderite reflect a biologic component to the ferrous Fe that was thought to exist in the deeper parts of these basins? Does biologically mediated precipitation of magnetite and hematite produce the relatively high δ^{56}Fe values of these oxides that are observed in the BIFs? Can we extract the δ^{56}Fe value of the Fe-rich Archean oceans from these results, and how has this varied over geologic time?

Although new Fe isotope data on BIFs raise many new questions that we cannot yet conclusively answer, these results demonstrate that significant Fe isotope variations may be preserved in ancient sedimentary rocks. This observation provides a clear motivation for detailed experimental calibration of equilibrium Fe isotope fractionations at low temperatures for minerals that are pertinent to surface and near-surface environments.

6. Conclusions and future directions

It is now possible to analyze Fe isotope compositions to a sufficiently high precision (±0.2‰ to ±0.05‰ for ^{56}Fe/^{54}Fe; depending on the method) that it is possible to identify naturally occurring, mass-dependent isotope variations. So far, δ^{56}Fe values for rocks, minerals, and aqueous species from low-temperature natural environments appear to vary by 3.5‰. In contrast, δ^{56}Fe values of a wide variety of igneous rocks from oceanic and continental settings are homogenous within analytical error, providing an exceptional isotopic baseline from which to compare Fe isotope compositions from low-temperature systems. The "constancy" in Fe isotope compositions of igneous Fe places major constraints on the possible range in "initial" isotopic compositions for biotic and abiologic processes and stands in marked contrast to the light stable isotope systems such as H, C, and O. It is yet unclear if the restriction of anomalous δ^{56}Fe values to low-temperature environments largely reflects abiological isotope fractionation between minerals and fluids, a biologic influence, or both.

Interpretation of the causes of naturally occurring Fe isotope variations, however, is difficult at present because very little is known concerning the controls of Fe isotope variations. Present-day iron isotope studies are in much the same position as oxygen isotope studies of the 1950s; the analytical tools to make isotope measurements have just become available, but the experimental database for equilibrium and kinetic Fe isotope fractionation factors in geologically meaningful systems has only just begun to be assembled. Theoretical calculations on the magnitude of equili-

brium Fe isotope fractionation factors (Polyakov, 1997; Polyakov and Mineev, 2000; Schauble et al., 2001) may provide useful predictive tools, but have yet to be confirmed by experimental measurements, and in two cases do not match experimental values. For example, the significant Fe isotope variations we have measured for Banded Iron Formations can be variably interpreted to represent inorganic equilibrium Fe isotope fractionation between magnetite and siderite, "vital" fractionation effects produced by organisms, or kinetic isotope fractionations produced by precipitation of Fe from Archean ocean water.

We have made some progress with the many experimental investigations that will be required to interpret Fe isotope data. Experimental data are most meaningful if they are cast in a clear kinetic or equilibrium context, and, drawing upon lessons form the light stable isotope literature, this can be achieved using enriched isotope tracers. Moreover, enriched tracer experiments allow one to quantify isotopic exchange rates for specific experiments. These reaction rates can be used to determine fluxes over time in synthesis experiments and evaluate complications that may arise during separation of aqueous species. Equilibrium isotope fractionation between $[Fe^{III}(H_2O)_6]^{3+}$ and $[Fe^{II}(H_2O)_6]^{2+}$ at 22 °C is +2.75‰ for $^{56}Fe/^{54}Fe$ ratios, which is approximately half that predicted from spectroscopic data. At 98 °C, isotope fractionation between $[Fe^{III}(H_2O)_6]^{3+}$ and hematite is very close to zero, suggesting that hematite may be useful in inferring the $\delta^{56}Fe$ values of ancient fluids. It seems clear, however, that many more experimental studies are required for aqueous and mineral systems before Fe isotope variations in natural minerals and fluids may be understood.

Acknowledgements

This research was supported by NSF grants EAR-9905436 and EAR-9903252, the NASA Astrobiology Institute, and funds from the University of Wisconsin-Madison Graduate School and Department of Geology and Geophysics. We wish to thank Nic Beukes, Cornelius Klein, and Julie O'Leary, for the numerous discussions and sharing their unpublished data. We thank S. Main and Z. Palacz of Micromass UK for aid in MC-ICP-MS developmental work. We also thank Darren Hutchenson of Micromass, for his expert instruction on operation of the *IsoProbe* during his installation of the instrument in the spring of 2000. Rebecca Poulson performed many of the Fe ion-exchange separations on igneous rocks. We are grateful to Bill White, who supplied many of the oceanic igneous rock samples. T. Bullen, S. Brantley, T. Lyons, and an anonymous reviewer are thanked for the comments on earlier versions of the paper. **[EO]**

References

Abouchami, W., Galer, S.J.G., Koschinsky, A., 1999. Pb and Nd isotopes in NE Atlantic Fe–Mn crusts: proxies for trace metal paleosources and paleocean circulation. Geochim. Cosmochim. Acta 63, 1489–1505.

Anbar, A.D., Roe, J.E., Barling, J., Nealson, K.H., 2000. Nonbiological fractionation of iron isotopes. Science 288, 126–128.

Bao, H., Koch, P.L., 1999. Oxygen isotope fractionation in ferric oxide–water systems: low temperature synthesis. Geochim. Cosmochim. Acta 63, 599–613.

Beard, B.L., Johnson, C.M., 1999. High precision iron isotope measurements of terrestrial and lunar materials. Geochim. Cosmochim. Acta 63, 1653–1660.

Beard, B.L., Johnson, C.M., Cox, L., Sun, H., Nealson, K.H., Aguilar, C., 1999. Iron isotope biosignatures. Science 285, 1889–1892.

Belshaw, N.S., Zhu, X.K., Guo, Y., O'Nions, R.K., 2000. High precision measurement of iron isotopes by plasma source mass spectrometry. Int. J. Mass Spectrom. 197, 191–195.

Beukes, N.J., 1983. Palaeoenvironmental setting of iron-formations in the depositional basin of the Transvaal Supergroup, South Africa. In: Trendall, A.F., Morris, R.C. (Eds.), Iron Formations: Facts and Problems. Elsevier, Amsterdam, pp. 131–209.

Beukes, N.J., Klein, C., 1990. Geochemistry and sedimentology of a facies transition from microbanded to granular iron-formation—in the early Proterozoic Transvaal Supergroup, South Africa. Precambrian Res. 47, 99–139.

Beukes, N.J., Klein, C., Kaufman, A.J., Hayes, J.M., 1990. Carbonate petrography, kerogen distribution, and carbon and oxygen isotope variations in an Early Proterozoic transition from limestone to iron-formation deposition, Transvaal Supergroup, South Africa. Econ. Geol. 85, 663–690.

Bidinosti, D.H., McIntyre, M.S., 1967. Electron-impact study of some binary metal carbonyls. Can. J. Chem. 3, 641–648.

Bjerrum, J., Lukeš, I., 1986. The iron(III) chloride system—a study of the stability constants and of the distribution of the tetrachloro species between organic solvents and aqueous chloride solutions. Acta Chem. Scand., A Phys. Inorg. Chem. 40, 31–40.

Brantley, S.L., Liermann, L., Bullen, T.D., 2001. Fractionation of Fe isotopes by soil microbes and organic acids. Geology 29, 535–538.

Brown, D.A., Gross, G.A., Sawicki, J.A., 1995. A review of the microbial geochemistry of banded iron-formations. Can. Min. 33, 1321–1333.

Bullen, T.D., McMahon, P.M., 1998. Using stable Fe isotopes to asses microbially mediated Fe3+ reduction in a jet-fuel contaminated aquifer. Min. Mag. 62A, 255–256.

Bullen, T.D., White, A.F., Childs, C.W., Vivit, D.V., Schulz, M.S., 2001. Demonstration of significant abiotic iron isotope fractionation in nature. Geology 29, 699–702.

Chako, T., Cole, D.R., Horita, J., 2001. Equilibrium oxygen, hydrogen, and carbon isotope fractionation factors applicable to geological systems. In: Valley, J.W., Cole, D.R. (Eds.), Stable Isotopes Geochemistry. Reviews in Mineralogy and Geochemistry, vol. 43. Mineralogical Society of America, Washington, D.C., pp. 1–81.

Cloud, P.E., 1965. Significance of the Gunflint (Precambrian) microflora. Science 148, 27–45.

Cole, D.R., Chakraborty, S., 2001. Rates and mechanisms of isotope exchange. In: Valley, J.W., Cole, D.R. (Eds.), Stable Isotopes Geochemistry. Reviews in Mineralogy and Geochemistry, vol. 43. Mineralogical Society of America, Washington, D.C., pp. 83–224.

Cole, D.R., Ohmoto, H., 1986. Kinetics of isotopic exchange at elevated temperatures and pressures. In: Valley, J.W., Taylor Jr., J.R., O'Neil, J.R. (Eds.), Stable Isotopes in High Temperature Geological Processes. Reviews in Mineralogy, vol. 16. Mineralogical Society of America, Washington, D.C., pp. 41–90.

Cornell, R.M., Schwertmann, U., 1996. The Iron Oxides Structure, Properties, Reactions, Occurrence and Uses VCH Publishers, New York. 573 pp.

Criss, R.E., 1999. Principles of Stable Isotope Distribution Oxford Univ. Press, New York. 254 pp.

Dixon, P.R., Janecky, D.R., Perrin, R.E., Rokop, D.J., Maeck, R., Janecky, D.R., Banar, J.P., 1993. Measurements of iron isotopes (^{54}Fe, ^{56}Fe, ^{57}Fe, ^{58}Fe) in submicrogram quantities of iron. Anal. Chem. 65, 2125–2130.

Doug, H.C., Frederickson, J.K., Kennedy, D.W., Zachara, J.M., Kukkadapu, D.W., Onstott, T.C., 2000. Mineral transformation associated with microbial reduction of magnetite. Chem. Geol. 169, 299–318.

Dymond, J., Lyle, M., Finney, B., Piper, D.Z., Murphy, K., Conrad, R., Pisias, N., 1984. Ferromanganese nodules from MANOP sites H, S, and R-control of mineralogic and chemical composition by multiple accretionary processes. Geochim. Cosmochim. Acta 48, 931–949.

Ehrlich, H.L., 1996. Geomicrobiology, 3rd ed. Marcel Dekker, New York, NY. 719 pp.

Finney, B., Heath, G.R., Lyle, M., 1984. Growth rates of manganese-rich nodules at MANOP site H (Eastern north Pacific). Geochim. Cosmochim. Acta 48, 911–919.

Forsythe, J.H., Maurice, P.A., Hersman, L.E., 1998. Attachment of *Pseudomonas* sp. to Fe(III)-(hydr)oxide surfaces. Geomicrobiol. J. 15, 293–308.

Gespard, S., Vazques, F., Holliger, C., 1998. Localization and solubilization of the Fe(II) reductase of *Geobacter sulfurreducens*. Appl. Environ. Microbiol. 64, 3188–3194.

Gledhill, M., van den Berg, C.M.G., 1995. Measurement of the redox speciation of iron in seawater by catalytic cathodic stripping voltammetry. Mar. Chem. 50, 51–61.

Gross, G.A., 1965. Geology of iron deposits in Canada—general geology and evaluation of deposits. Geol. Surv. Canada Report 22, vol. 1. 181 pp.

Hayes, J.M., 2001. Fractionation of carbon and hydrogen isotopes in biosynthetic processes. In: Valley, J.W., Cole, D.R. (Eds.), Stable Isotopes Geochemistry. Reviews in Mineralogy and Geochemistry, vol. 43. Mineralogical Society of America, Washington, D.C., pp. 225–278.

Herzog, G.F., Xue, S., Hall, G.S., Nyquist, L.E., Shih, C.-Y., Wiesmann, H., Brownlee, D.E., 1999. Isotopic and elemental composition of iron, nickel, and chromium, in type I deep-sea spherules: implications for origin and composition of the parent micrometeoroids. Geochim. Cosmochim. Acta 63, 1443–1457.

Hudson, R.J.M., Morel, F.M.M., 1989. Distinguishing between extra- and intracellular iron in marine phytoplankton. Limnol. Oceanogr. 34, 1113–1120.

Hudson, R.J.M., Morel, F.M.M., 1990. Iron transport in marine phytoplankton: kinetics of cellular and medium coordination reactions. Limnol. Oceanogr. 35, 1002–1020.

Hudson, R.J.M., Covault, D.T., Morel, F.M.M., 1992. Investigations of iron coordination and redox reactions in seawater using ^{59}Fe radiometry and ion-pair solvent extraction of amphiphilic iron complexes. Mar. Chem. 38, 209–235.

Isley, A.E., 1995. Hydrothermal plumes and the delivery of iron to banded iron formation. J. Geol. 103, 169–185.

James, H.L., 1954. Sedimentary facies of iron-formations. Econ. Geol. 49, 235–284.

James, H.L., 1983. Distribution of banded iron-formation in space and time. In: Trendall, A.F., Morris, R.C. (Eds.), Iron Formations: Facts and Problems. Elsevier, Amsterdam, pp. 471–490.

Johnson, C.M., Beard, B.L., 1999. Correction of instrumentally produced mass fractionation during isotopic analysis of Fe by thermal ionization mass spectrometry. Int. J. Mass Spectrom. 193, 87–99.

Johnson, T.M., Herbel, M.J., Bullen, T.D., Zawislanski, P.T., 1999. Selenium isotope ratios as indicators of selenium sources and oxyanion reduction. Geochim. Cosmochim. Acta 63, 2775–2783.

Johnson, C.M., Skulan, J.L., Beard, B.L., Sun, H., Nealson, K.H., Braterman, P.S., 2002. Isotopic fractionation between Fe(III) and Fe(II) in aqueous solutions. Earth Planet. Sci. Lett. 195, 141–153.

Johnson, C.M., Beard, B.L., Beukes, N.J., Klein, C., O'Leary, J.M., 2003. Ancient geochemical cycling in the earth as inferred from Fe isotope studies of bandied Iron formations from the Transvaal Craton. Contrib. Mineral. Petrol., in press.

Kim, S.-T., O'Neil, J.R., 1997. Equilibrium and nonequilibrium oxygen isotope effects in synthetic carbonates. Geochim. Cosmochim. Acta 61, 3461–3475.

Klein, C., Beukes, N.J., 1989. Geochemistry and sedimentology of a facies transition from limestone to iron-formation deposition in the early Proterozoic Transvaal Supergroup, South Africa. Econ. Geol. 84, 1733–1774.

Klein, C., Beukes, N.J., 1992. Time distribution, stratigraphy, and sedimentologic setting, and geochemistry of precambrian iron-

formations. In: Schopf, J.W., Klein, C. (Eds.), The Proterozoic Biosphere: A Multidisciplinary Study. Cambridge Univ. Press, New York, pp. 139–146.

Kraus, K.A., Nelson, F., 1956. Anion exchange studies of the fission products. Proc. U. N. Int. Conf. Peaceful Uses At. Energy, 1st 7, 113–125.

Lovley, D.R., 1991. Dissimilatory Fe(III) and Mn(IV) reduction. Microbiol. Rev. 55, 259–287.

Mandernack, K.W., Bazylinski, D.A., Shanks III, W.C., Bullen, T.D. 1999. Oxygen and iron isotope studies of magnetite produced by magnetotactic bacteria. Science 285, 1892–1896.

Maranger, R., Bird, D.F., Price, N.M., 1998. Iron acquisition by photosynthetic marine phytoplankton from ingested bacteria. Nature 396, 248–251.

Marechal, C.N., Philippe, T., Albarede, F., 1999. Precise analysis of copper and zinc isotopic compositions by plasma-source mass spectrometry. Chem. Geol. 156, 251–273.

Matsuhisa, Y., Goldsmith, J.R., Clayton, R.N., 1978. Mechanism of hydrothermal recrystallization of quartz at 250 °C and 15 kb. Geochim. Cosmochim. Acta 42, 173–183.

Matthews, A., Zhu, X.-K., O'Nions, R.K., 2001. Kinetic iron stable isotope fractionation between iron (-II) and iron (-III) complexes in solution. Earth Planet. Sci. Lett. 192, 81–92.

McConnaughey, T., 1989. ^{13}C and ^{18}O isotopic disequilibrium in biological carbonates: I. Patterns. Geochim. Cosmochim. Acta 53, 151–162.

Millero, F.J., Yao, W., Aicher, J., 1995. The speciation of Fe(II) and Fe(III) in natural waters. Mar. Chem. 50, 21–39.

Miyano, T., Beukes, N.J., 1984. Phase relations of stilpnomelane, ferri-annite, and riebeckite in very low grade metamorphosed iron formations. Trans. Geol. Soc. S. Afr. 87, 111–124.

Myers, C.R., Nealson, K.H., 1988. Bacterial manganese reduction and growth with manganese oxide as the sole electron-acceptor. Science 240, 1319–1321.

Nealson, K., 1983. The microbial Fe cycle. In: Krumbein, E. (Ed.), Microbial Biogeochemistry. Blackwell, Oxford, pp. 159–190.

Nealson, K.H., Myers, C.R., 1990. Iron reduction by bacteria: a potential role in the genesis of banded iron formations. Am. J. Sci. 290, 35–45.

Nealson, K.H., Myers, C., 1992. Microbial reduction of manganese and iron: new approaches to carbon cycling. Appl. Environ. Microbiol. 58, 439–443.

Nealson, K.H., Stahl, D.A., 1997. Microorganisms and biogeochemical cycles: what can we learn from layered microbial communities. In: Banfield, J.F., Nealson, K.H. (Eds.), Geomicrobiology: Interactions Between Microbes and Minerals. Reviews in Mineralogy, vol. 35. Mineralogical Society of America, Washington, D.C., pp. 5–34.

Nevin, K.P., Lovley, D.R., 2000. Lack of production of electron-shuttling compounds or solubilization of Fe(III) during reduction of insoluble Fe(III) oxide by *Geobacter metallireducens*. Appl. Environ. Microbiol. 66, 2248–2251.

Newmann, D.K., Kolter, R., 2000. A role for excreted quinones in extracellular electron transfer. Nature 405, 94–97.

Northrop, D.A., Clayton, R.N., 1966. Oxygen isotope fractionations in systems containing dolomite. J. Geol. 74, 174–196.

O'Neil, J.R., 1986. Theoretical and experimental aspects of isotopic fractionation. In: Valley, J.W., Taylor Jr., H.P., O'Neil, J.R. (Eds.), Stable Isotopes in High Temperature Geological Processes. Reviews in Mineralogy, vol. 16. Mineralogical Society of America, Washington, D.C., pp. 1–40.

O'Nions, R.K., Frank, M., von Blackenburg, F., Ling, H.F., 1998. Secular variation of Nd and Pb isotopes in ferromanganese crusts from the Atlantic, Indian, and Pacific oceans. Earth Planet. Sci. Lett. 155, 15–28.

Polyakov, V.B., 1997. Equilibrium fractionation of the iron isotopes: estimation from Moessbauer spectroscopy data. Geochim. Cosmochim. Acta 61, 4213–4217.

Polyakov, V.B., Mineev, S.D., 2000. The use of Mössbauer spectroscopy in stable isotope geochemistry. Geochim. Cosmochim. Acta 64, 849–865.

Ravelo, A.C., Fairbanks, R.G., 1995. Carbon isotopic fractionation in multiple species of planktonic foraminifera from core-tops in the tropical Atlantic. J. Foraminiferal Res. 25, 53–74.

Russell, W.A., Papanastassiou, D.A., Tombrello, T.A., 1978. Ca isotope fractionation on the Earth and other solar system materials. Geochim. Cosmochim. Acta 42, 1075–1090.

Schauble, E.A., Rossman, G.R., Taylor, H.P., 2001. Theoretical estimates of equilibrium Fe-isotope fractionations from vibrational spectroscopy. Geochim. Cosmochim. Acta 65, 2487–2497.

Schidlowski, M., Hayes, J.M., Kaplan, I.R., 1983. Isotopic references of ancient biochemistries: carbon, sulfur, hydrogen and nitrogen. In: Schopf, J.W. (Ed.), Earth's Earliest Biosphere: Its Origin and Evolution. Princeton Univ. Press, NJ, pp. 149–186.

Schwertmann, U., Cornell, R.M., 1991. Iron Oxides in the Laboratory: Preparation and Characterization Weinheim. VCH Publishers, Weinheim, Germany. 137 pp.

Skulan, J.L., Beard, B.L., Johnson, C.M., 2002. Kinetic and equilibrium Fe isotope fractionation between aqueous Fe(III) and hematite. Geochim. Cosmochim. Acta 66, 2995–3015.

Stookey, L.C., 1970. Ferrozine—a new spectrophotometric reagent for iron. Anal. Chem. 42, 779–781.

Strelow, F.W.E., 1980. Improved separation of iron from copper and other elements by anion-exchange chromatography on a 4% cross-linkage resin with high concentrations of hydrochloric acid. Tatlanta 27, 727–732.

Takeda, S., Obata, H., 1995. Response of equatorial Pacific phytoplankton to subnanomolar Fe enrichment. Mar. Chem. 50, 219–227.

Taylor, P.D.P., Maeck, R., De Bièvre, P., 1992. Determination of the absolute isotopic composition and atomic weight of a reference sample of natural iron. Int. J. Mass Spectrom. Ion Process. 121, 111–125.

Taylor, P.D.P., Valkiers, S., De Bièvre, P., 1993a. Stable isotope analysis of iron by gas-phase electron impact mass spectrometry. Anal. Chem. 65, 3166–3167.

Taylor, P.D.P., Maeck, R., Hendrickx, F., De Bièvre, P., 1993b. The gravimetric preparation of synthetic mixtures of iron isotopes. Int. J. Mass Spectrom. Ion Process. 128, 91–97.

Trautani, T., Clayton, R.N., Maydea, T.K., 1969. The effect of polymorphism and magnesium substitution on oxygen isotope fractionation between calcium carbonates and water. Geochim. Cosmochim. Acta 33, 987–996.

Trendall, A.F., 1968. Three great basins of precambrian banded iron

formation deposition: a systematic comparison. Bull. Geol. Soc. Am. 79, 1527–1544.

Trendall, A.F., 1983. Introduction. In: Trendall, A.F., Morris, R.C. (Eds.), Iron Formations: Facts and problems. Elsevier, Amsterdam, pp. 1–12.

Trendall, A.F., Blockley, J.G., 1970. The iron formations of the Precambrian Hamersley Group, Western Australia. Bull.-Geol. Surv. West. Aust. 119 (366 pp.).

Tugel, J.B., Hines, M.E., Jones, G.E., 1986. Microbial iron reduction by enrichment cultures isolated from estuarine waters. Appl. Environ. Microbiol. 52, 1167–1172.

Turner, J.V., 1982. Kinetic fractionation of carbon-13 during calcium carbonate precipitation. Geochim. Cosmochim. Acta 46, 1183–1191.

Urey, H.C., Lowenstam, H.A., Epstein, S., McKinney, C.R., 1951. Measurement of paleotemperatures and temperatures of the Upper Cretaceous of England, Denmark, and the southeastern United States. Bull. Geol. Soc. Am. 62, 399–416.

van den Berg, C.M.G., 1995. Evidence for organic complexation of iron in seawater. Mar. Chem. 50, 139–157.

Völkening, J., Papanastassiou, D.A., 1989. Iron isotope anomalies. Astrophys. J. 347, L43–L46.

Walczyk, T., 1997. Iron isotope ratio measurements by negative thermal ionization mass spectrometry using FeF4-molecular ions. Int. J. Mass Spectrom. Ion Process. 161, 217–227.

Widdel, F., Schnell, S., Heising, S., Ehernreich, A., Assmus, B., Schink, B., 1993. Ferrous iron oxidation by anoxygenic phototrophic bacteria. Science 362, 834–836.

Zhu, X.K., O'Nions, R.K., Guo, Y., Reynolds, B.C., 2000. Secular variation of iron isotopes in north Atlantic Deep Water. Science 287, 2000–2002.

Zhu, X.K., Guo, Y., O'Nions, R.K., Young, E.D., Ash, R.D., 2001. Isotopic homogeneity of iron in the early solar nebula. Nature 412, 311–313.